



Robust adaptive flexible prescribed performance tracking and vibration control for rigid–flexible coupled robotic systems with input quantization

Xingyu Zhou · Haoping Wang  · Yang Tian

Received: 21 July 2023 / Accepted: 24 November 2023 / Published online: 26 December 2023
© The Author(s), under exclusive licence to Springer Nature B.V. 2023

Abstract With the increasing demands for more flexibility, lighter weight, and larger working space of industrial robotic systems in many fields, the rigid–flexible coupled robotic systems attract more attention. In this work, the desired angular tracking and vibration suppression issues are investigated for the rigid–flexible coupled robotic systems (RFCRSs) in the presence of input quantization. The vibrating displacement is coupled nonlinear due to the coupling between two joints’ angular positions and flexible displacements. Using the assumed mode principle, the nonlinear infinite-dimension dynamics of rigid–flexible coupled robotic systems are reduced by ordinary differential equations. With the backstepping-based Lyapunov method, robust adaptive flexible prescribed performance control (FPPC) law is developed to track the given angular positions and to reduce the vibration oscillations. Besides, the robust adaptive update law is incorporated into the quantized FPPC for estimating the unknown parameters of logarithmic quantizers in the face of input quantization. In terms of the above robust adaptive FPPC control, the tracking errors of the RFCRSs eventually converge to a compact set in face

of input quantization. At last, three comparison cases are implemented to verify the efficacy of the proposed robust adaptive FPPC strategy in comparison with the PD feedback law.

Keywords Rigid–flexible coupled robotic systems · Flexible prescribed performance tracking control · Logarithmic quantizer · Vibration suppression · Stability analysis

1 Introduction

Rigid–flexible coupled robotic systems (RFCRSs) have attracted wide attention spurred by the rapid development of aerospace [1–3], marine engineering [4,5], and modern medical technology [6,7]. In general, the RFCRSs comprise a rigid link connected to a flexible link and are driven by the joint motor. Compared with the conventional rigid robotic system, the above RFCRSs are comparatively more agile and lighter [8]. However, the significant flaw of the RFCRSs mechanics is that the flexible beam is vulnerable to producing the flexible vibration that often leads to poor operational performance [9]. Hence, there are urgent requirements for vibration elimination of RFCRSs to prevent destruction and guarantee successful operation [10].

In reality, the elastic vibration of RFCRSs involves not only the time variable but also the spatial variable. Mathematically, RFCRSs can be described as distributed parameter systems governed by partial dif-

X. Zhou
School of Electrical Engineering, Nantong University, Nantong
226019, Jiangsu, People’s Republic of China

X. Zhou · H. Wang (✉) · Y. Tian
LaFCAS, School of Automation, Nanjing University of Science
and Technology, Nanjing 210094, Jiangsu, People’s Republic of
China
e-mail: hp.wang@njust.edu.cn

ferential equations (PDEs). To be candid, modeling and analyzing precise dynamic equations for RFCRSs is a formidable challenge. This is primarily due to the extreme difficulty in solving exact solutions for the dynamics of infinite-dimensional systems, and the inherent complexity of PDEs presents significant obstacles and limitations in the development of vibration control strategies [11]. While there are control approaches designed to address the dynamic model of PDEs and tackle these challenges [12–14], many of these methods require the installation of an input force at the endpoint of the flexible structure to dampen vibrations. Unfortunately, implementing such a solution is often challenging, especially on the majority of industrial robots [15].

More recently, the reduced-model method which includes finite element methods, assumed mode method, and lumped parameter method, has been widely applied to transform PDEs into ordinary differential equations (ODEs) [16–18]. For instance, adopting the lumped spring-mass model, a flexible robotic mechanism with uncertain dynamics was controlled by an adaptive neural network (NN). [19]. By using the assumed mode method (AMM), a disturbance observer was added to the NN control for the reduced dynamics of a flexible beam to cope with unknown spatiotemporally variable disturbances in [20]. Based on the AMM, a planar two-link rigid–flexible manipulator was modeled by the reduced ODEs, and the uncalibrated visual servoing method was proposed subject to joint-space-velocity measurement [17]. A sliding mode control law-based adaptive tracking controller was put forward in [21] to enable an uncertain two-link rigid–flexible manipulator to achieve the necessary angles while being constrained by vibration amplitude. The existing studies on RFCRSs governed by PDEs principally handle the issues of input constraints though a barrier Lyapunov function, which is extensively applied to handle the output or state constraints, is investigated in [9, 13] to follow the given positions and suppress flexible displacements concurrently.

However, the prescribed performance functions selected in most references [23–26] can only be appended to exponential functions with symmetric features, which belong to the conventional prescribed performance scheme. Actually, the dynamic and steady-state process with the aforementioned scheme is still on the basis of intrinsic characterizes of the control input design (semi-global/global converge approach)

[27, 28]. Therefore, the traditional performance functions have certain restrictions and lack flexibility. In this work, a more relatively flexible situation, where the steady-state performance of tracking errors relies on a flexible performance function [29], is concerned. The aforesaid literature on the RFCRSs did not consider the input quantization topic which is an inevitable issue in industrial control [30–32].

With the rapid development of network techniques, the integration of communication and control with the use of digital communication has triggered mounting research attention [33–38]. The input quantization is a core problem that usually combines with modern control methods to transform the control signal's domain, which is continuous, into one that is discrete. The tradeoff between the controlled system stability and the admissible control precision has become more significant on account of quantization errors. Taking into account the input quantization of the RFCRSs which leads to the appearance of system instability makes the control issue of such rigid–flexible coupled systems relatively difficult [36, 37]. In the existing research on the RFCRSs, an adaptive boundary control with input signal quantization was proposed in three-dimensional space for an Euler–Bernoulli beam, and quantitative logarithmic laws were used to eliminate the elastic vibrations in [36]. With the help of the PDEs model, a feedback boundary quantized control law was designed to realize both joint angle tracking and vibration repression [37]. In comparison with the control issues in [36] and [37], the flexible prescribed performance of tracking errors case is considered in our work where the predefined flexible performance functions can be arbitrarily selected.

To construct the dynamic equation of RFCRSs and address the aforementioned difficulties, the reduced-model approach (AMM) is implemented and a novel flexible prescribed performance tracking approach with input quantization is proposed for such robotic systems. The main innovations of this work, as compared to previous research, include:

1. Unlike the traditional barrier Lyapunov functions, a novel parameter-type Lyapunov function is proposed in this paper. By virtue of constructing the parameter function $\Pi(t)$, the both dynamic and steady-state performance of tracking errors rely on the flexible prescribed performance functions.

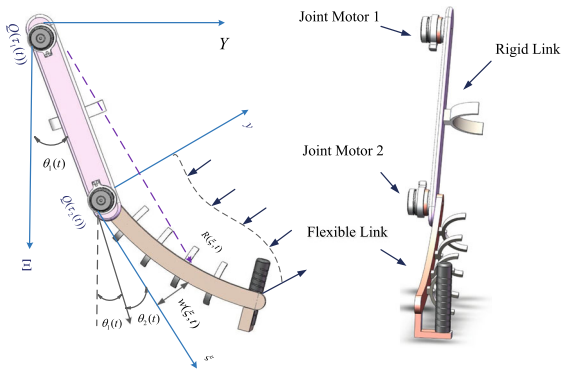


Fig. 1 Basic structure diagram of RFCRSs

2. A hybrid flexible prescribed performance controller (FPPC) with a robust adaptive parameter compensation scheme is developed. It is confirmed by backstepping-based Lyapunov’s stability and three numerical comparisons that input quantization-induced flexible vibrations and regulation of output errors will ultimately converge to zero over a compact neighborhood.

The rest of the article is organized as follows. In Sect. 2, the reduced dynamic equations and problem statements for RFCRSs are presented. A novel FPPC scheme is proposed via the backstepping method in the face of quantized input signals in Sect. 3. Three numerical simulations are shown in Sect. 4 and conclusions are made in Sect. 5.

2 Dynamic modeling and control objectives of RFCRSs

The fundamental structural components of RFCRSs consist of two links, as illustrated in Fig. 1. The first and second links of the RFCRS, located above the horizontal plane, are rigid and flexible, respectively. It is commonly assumed that the second link is modeled as an Euler–Bernoulli beam with a length of l_2 . The coordinate axis of inertia is denoted as $\mathcal{E} O Y$, while the local rotating reference frame mounted at hub O is represented as $\xi O y$. The angular positions of the two joints, with $i = 1, 2$, are denoted by $\theta_i(t)$. The elastic displacement of the flexible link at a given position ξ and time is denoted as $w(\xi, t)$. The control inputs for this RFCRS, described by $\tau_i(t)$, $i = 1, 2$, represent the joint torques. Additional characteristics of RFCRSs are presented in Table 1.

Table 1 Feature parameter configuration of RFCRSs

Items	Meaning	Values	Unit
EI	Uniform flexural rigidity	3	Nm ²
M_h	Mass about joint	0.2	kg
M_t	Mass about tip payload	0.3	kg
ρ	Mass density per unit	0.4	kg/m
l_1	1st link length	0.5	m
l_2	2nd link length	0.8	m
J_1	rigid link inertia	0.0625	kgm ²
I_h	flexible link inertia	0.042	kgm ²

Remark 1 For ease of understanding, the following sections make use of these notations $(*)' = \partial(*)/\partial\xi$, $(*)'' = \partial^2(*)/\partial\xi^2$, $(*)\dot{=} \partial(*)/\partial t$, $(*)\ddot{=} \partial^3(*)/\partial t^3$.

2.1 Dynamics formula of RFCRSs via energy analysis

The following dynamic equations are derivable from the energy analysis of RFCRSs using the expanded Hamilton’s principle [9, 22].

These are the angular positions $\theta(t)$ for which the dynamic model is given:

$$M(\omega(\xi, t), \theta)\ddot{\theta}(t) + C(\dot{\omega}(\xi, t), \theta(t))\dot{\theta}(t) + G(\theta(t), \dot{\theta}, \dot{\omega}(\xi, t), \ddot{\omega}(\xi, t)) = \mathcal{Q}(\tau(t)) \tag{1}$$

Considered is the dynamic formula for the vibration displacement $w(\xi, t)$:

$$\begin{aligned} &\rho \int_0^{l_2} [\ddot{w}(\xi, t) + l_1(\dot{\theta}_1^2 \sin \theta_2 + \ddot{\theta}_1 \cos \theta_2) + \xi(\ddot{\theta}_1 + \ddot{\theta}_2) + \omega(\xi, t)(\dot{\theta}_1 + \dot{\theta}_2)^2] d\xi + EI \int_0^{l_2} \omega''''(\xi, t) d\xi + M_t \ddot{w}(l_2, t) \\ &+ M_t l_1 (\dot{\theta}_1^2 \sin \theta_2 + \ddot{\theta}_1 \cos \theta_2) + M_t l_2 (\ddot{\theta}_1 + \ddot{\theta}_2) - M_t \omega(l_2, t) (\dot{\theta}_1 + \dot{\theta}_2)^2 = 0. \end{aligned} \tag{2}$$

The following boundary conditions apply to them:

$$w''(l_2, 0) = w'''(l_2, 0) = 0, \tag{3}$$

$$w(0, t) = w'(0, t) = 0, \tag{4}$$

Remark 2 For the sake of simplicity and to facilitate the explanation of the subsequent reduced-order technique for infinite-dimensional systems, detailed information about the parameter matrices, such as $M(\omega(\xi, t), \theta)$, $C(\dot{\omega}(\xi, t), \theta(t))$, $G(\dot{\omega}(\xi, t), \theta(t), \dot{\theta}(t))$, has been

omitted in this section but can be found in our previous works [9, 22]. Additionally, $\mathcal{Q}(\tau(t))$ represents the quantized input signal of $\tau(t)$, which will be elaborated upon in the following section.

2.2 Reduced-order finite-dimensional dynamic model of RFCRSs

The aforementioned approach AMM is used to convert the infinite-dimension system model governed by PDEs into ODEs. The dynamic equations are usually truncated to some finite-dimensional models with the use of the assumed mode method (AMM). For the AMM, the elastic deflection is usually represented by an infinite number of separable harmonic modes theoretically, but practically only a finite number of modes with comparatively low frequencies are considered as they are generally dominant in the system dynamic behavior.

The method of arc approximation is used to represent the vibration displacement of the flexible link, which leads to the finite dimensional reduced-order dynamics. Following is a description of the vibration displacement of the flexible portion $w(\xi, t)$.

$$w(\xi, t) = \sum_{i=1}^N \phi_i(\xi)q_i(t) \tag{5}$$

where the i th shape of the mode function is denoted by $\phi_i(\xi)$ and the i th generalized mode coordinate is represented by $q_i(t)$.

The i th mode shape function $\phi_i(\xi)$ is presented in [18] as

$$\begin{aligned} \phi_i(\xi) &= \frac{1}{\mathcal{E}_i} [-\gamma_i (\sinh(\lambda_i \xi) - \sin(\lambda_i \xi)) \\ &\quad + \cosh(\lambda_i \xi) - \cos(\lambda_i \xi)] \\ \gamma_i &= \frac{\cosh(\lambda_i l_2) + \cos(\lambda_i l_2)}{\sin(\lambda_i l_2) + \sinh(\lambda_i l_2)}, \end{aligned}$$

where if $M_t = 0$, then $\mathcal{E}_i = \sqrt{l_2}$; otherwise,

$$\mathcal{E}_i = \left[l_2 + \frac{EI}{M_t \lambda_i^2} \left(\frac{1 + \cosh(\lambda_i l_2) \cos(\lambda_i l_2)}{\sinh(\lambda_i l_2) \sin(\lambda_i l_2)} \right)^2 \right]^{\frac{1}{2}}$$

and λ_i is the i th positive resolution such that

$$\begin{aligned} \frac{M_t \lambda_i}{EI l_2} [-\sin(\lambda_i) \cosh(\lambda_i) + \cos(\lambda_i) \sinh(\lambda_i)] \\ + \cosh(\lambda_i) \cos(\lambda_i) = -1. \end{aligned}$$

Remark 3 It ought to be noticed that the first two modes are adequate to represent how the flexible beam vibrates, which can also refer to [8]-[10]. Only the first two modes are taken into consideration in this work to simplify the structure of the proposed tracking and vibration control technique, that is $w(\xi, t) = q_1(t)\phi_1(\xi) + q_2(t)\phi_2(\xi)$.

The following vectors are utilized to recreate the finite-dimensional dynamic:

$$\begin{aligned} \tau(t) &= [\tau_1(t) \ \tau_2(t) \ 0 \ 0]^T \text{ and} \\ \Theta(t) &= [\theta_1(t) \ \theta_2(t) \ q_1(t) \ q_2(t)]^T. \end{aligned}$$

The dynamic equations of PDEs can be reduced into the form of ODEs by substituting (5) into (1) and (2), which could be described via the subsequent compact formula:

$$M\ddot{\Theta}(t) + K\Theta(t) + F(\Theta(t), \dot{\Theta}(t)) = \mathcal{Q}(\tau(t)) \tag{6}$$

where K represents a stiffness matrix and M specifies a positive-definite symmetric inertia matrix as follows:

$$K = \begin{bmatrix} 0 & 0 & 0 & 0 \\ 0 & 0 & 0 & 0 \\ 0 & 0 & k_1 & 0 \\ 0 & 0 & 0 & k_2 \end{bmatrix}, \quad k_i = EI \int_0^{l_2} [\phi_i''(\xi)]^2 d\xi, \quad i = 1, 2,$$

and $F(\Theta(t), \dot{\Theta}(t))$ which denotes a hybrid Coriolis and centrifugal matrix satisfies the following property

$$\begin{aligned} F(\Theta(t), \dot{\Theta}(t)) &= \frac{dM(\Theta(t))}{dt} \dot{\Theta}(t) - \frac{1}{2} \frac{\partial[\dot{\Theta}^T M(\Theta) \dot{\Theta}]}{\partial \Theta} \\ &= C(\Theta(t), \dot{\Theta}(t)) \dot{\Theta}(t) \end{aligned}$$

Following are a few notations that have been included for clarity:

$$\begin{cases} \sigma_i = \int_0^{l_2} \phi_i(\xi) d\xi, & \psi_i = \int_0^{l_2} \xi \cdot \phi_i(\xi) d\xi, \\ \eta_i = \int_0^{l_2} \phi_i^2(\xi) d\xi, & \text{with } i = 1, 2 \end{cases}$$

Following are specifics on the inertia matrix M :

$$\begin{aligned}
 M_{11} &= J_1 + I_h + M_h l_1^2 + \rho_2 l_1^2 l_2 + \frac{1}{3} \rho_2 l_2^3 \\
 &\quad + \rho_2 l_1 l_2^2 \cos \theta_2 - 2 l_1 \rho_2 \sin \theta_2 (q_2(t) \sigma_2 + q_1(t) \sigma_1) \\
 &\quad + M_t (l_1^2 + l_2^2) + \rho_2 l_2 (q_1^2(t) \eta_1 + q_2^2(t) \eta_2) \\
 &\quad + M_t [q_1^2(t) \phi_1^2(l_2) + l_1 l_2 \cos \theta_2 + q_2^2(t) \phi_2^2(l_2)] \\
 &\quad - 2 l_1 \sin \theta_2 (q_2(t) \phi_2(l_2) + q_1(t) \phi_1(l_2)) \\
 &\quad + 2 q_1(t) q_2(t) \phi_1^2(l_2) \phi_2^2(l_2) \\
 M_{12} &= I_h + \frac{1}{3} \rho_2 l_2^3 + \rho_2 (q_1^2(t) \eta_1 + q_2^2(t) \eta_2) \\
 &\quad + \frac{1}{2} \rho_2 l_1 l_2^2 \cos \theta_2 - \rho_2 l_1 \sin \theta_2 (q_1(t) \sigma_1 + q_2(t) \sigma_2) \\
 &\quad + M_t [l_2^2 + l_1 l_2 \cos \theta_2 - l_1 \sin \theta_2 (q_1(t) \phi_1(l_2) \\
 &\quad + q_2(t) \phi_2(l_2)) + q_1^2(t) \phi_1^2(l_2) \\
 &\quad + \phi_2^2(l_2) q_2^2(t) + 2 \phi_1(l_2) q_1(t) q_2(t) \phi_2(l_2)] \\
 M_{13} &= \rho \psi_1 + \rho l_1 \sigma_1 \cos \theta_2 + M_t l_1 \phi_1(l_2) \cos \theta_2 \\
 &\quad + M_t l_2 \phi_1(l_2) \\
 M_{14} &= \rho \psi_2 + \rho l_1 \sigma_2 \cos \theta_2 + M_t l_1 \phi_2(l_2) \cos \theta_2 \\
 &\quad + M_t l_2 \phi_2(l_2) \\
 M_{22} &= I_h + \frac{1}{3} \rho_2 l_2^3 + \rho_2 (q_1^2(t) \eta_1 + q_2^2(t) \eta_2) \\
 &\quad + q_2^2(t) \phi_2^2(l_2) \\
 &\quad + M_t [l_2^2 + q_1^2(t) \phi_1^2(l_2) + 2 \phi_1(l_2) q_2(t) q_1(t) \phi_2(l_2)] \\
 M_{23} &= \rho \psi_1 + M_t l_2 \phi_1(l_2); \quad M_{24} = \rho \psi_2 + M_t l_2 \phi_2(l_2) \\
 M_{33} &= \rho \eta_1 + M_t \phi_1^2(l_2); \quad M_{34} = \phi_2(l_2) \phi_1(l_2) M_t; \\
 M_{44} &= \rho \eta_2 + M_t \phi_2^2(l_2)
 \end{aligned}$$

and coriolis matrix's equivalent components are:

$$\begin{aligned}
 F_1(\Theta, \dot{\Theta}) &= \left[-\rho l_1 \sin \theta_2 l_2^2 + 2 \cos \theta_2 l_1 \rho \left(\sum_{i=1}^2 q_i(t) \sigma_i \right) \right. \\
 &\quad \left. - 2 \sin \theta_2 l_1 M_t l_2 + 2 \cos \theta_2 l_1 M_t \sum_{i=1}^2 q_i(t) \phi_i(l_2) \right] \dot{\theta}_1 \dot{\theta}_2 \\
 &\quad - \left[\rho l_1 \sin \theta_2 \frac{l_2^2}{2} + \cos \theta_2 l_1 \rho \left(\sum_{i=1}^2 \sigma_i q_i(t) \right) \right. \\
 &\quad \left. + M_t l_1 l_2 \sin \theta_2 + \cos \theta_2 l_1 M_t \sum_{i=1}^2 \phi_i(l_2) q_i(t) \right] \dot{\theta}_2^2 \\
 &\quad - \left[2 \rho \sin \theta_2 l_1 \sum_{i=1}^2 \dot{q}_i(t) \sigma_i - 2 \rho \sum_{i=1}^2 q_i(t) \eta_i \dot{q}_i(t) \right. \\
 &\quad \left. + 2 M_t l_1 \sin \theta_2 \sum_{i=1}^2 \dot{q}_i(t) \phi_i(l_2) \right]
 \end{aligned}$$

$$\begin{aligned}
 &\quad \left. - 2 M_t \sum_{i=1}^2 q_i(t) \phi_i(l_2) \sum_{i=1}^2 \dot{q}_i(t) \phi_i(l_2) \right] (\dot{\theta}_1 + \dot{\theta}_2) \\
 F_2(\Theta, \dot{\Theta}) &= \left[\rho l_1 \sin \theta_2 \frac{l_2^2}{2} + \cos \theta_2 l_1 \rho \left(\sum_{i=1}^2 \sigma_i q_i(t) \right) \right. \\
 &\quad \left. + M_t l_1 l_2 \sin \theta_2 + \cos \theta_2 l_1 M_t \sum_{i=1}^2 \phi_i(l_2) q_i(t) \right] \dot{\theta}_1^2 \\
 &\quad + 2 \rho \sum_{i=1}^2 q_i(t) \eta_i \dot{q}_i(t) \cdot (\dot{\theta}_1 + \dot{\theta}_2) \\
 &\quad + \left[2 M_t \sum_{i=1}^2 \phi_i(l_2) q_i(t) + \sum_{i=1}^2 \phi_i(l_2) \dot{q}_i(t) \right] \cdot (\dot{\theta}_1 + \dot{\theta}_2) \\
 F_3(\Theta, \dot{\Theta}) &= \rho q_1(t) \eta_1 l_2 (\dot{\theta}_1 + \dot{\theta}_2)^2 - \dot{\theta}_1^2 \rho l_1 \sin \theta_2 \sigma_1 \\
 &\quad + M_t (\dot{\theta}_1 + \dot{\theta}_2)^2 (\phi_1(l_2) q_2(t) \phi_2(l_2) + q_1(t) \phi_1^2(l_2)) \\
 &\quad + l_1 \dot{\theta}_1^2 \sin \theta_2 M_t \phi_1(l_2) \\
 F_4(\Theta, \dot{\Theta}) &= \rho q_2(t) \eta_2 l_2 (\dot{\theta}_1 + \dot{\theta}_2)^2 - \dot{\theta}_1^2 \rho l_1 \sin \theta_2 \sigma_2 \\
 &\quad + M_t (\dot{\theta}_1 + \dot{\theta}_2)^2 (\phi_2^2(l_2) q_2(t) + \phi_1(l_2) q_1(t) \phi_2(l_2)) \\
 &\quad + l_1 \dot{\theta}_1^2 \sin \theta_2 M_t \phi_2(l_2)
 \end{aligned}$$

2.3 Flexible prescribed performance control objectives

With the compact system described above, one can derive the equivalent formulation as follows:

$$\begin{cases} \dot{x}_1(t) = x_2(t), \\ \dot{x}_2(t) = M(x_1)^{-1} [\mathcal{Q}(\tau(t)) - Kx_1(t) - C(x_1, x_2)x_2(t)] \end{cases} \quad (7)$$

with $x_1(t) = \Theta(t)$ and $x_2(t) = \dot{\Theta}(t)$.

Concerning the RFCRSs (1) with prescribed performance, the flexible PPC law is developed via the backstepping-based Lyapunov strategy in the presence of quantization, so that the whole states of the closed-loop RFCRSs are semi-globally consistent and ultimately bounded under input quantization:

a) The tracking errors of two desired joint positions satisfy the prescribed performance, i.e., $e_i(t)$ meets $\mathcal{A}_i(t) < e_i(t) < \mathcal{B}_i(t)$ with $i = 1, 2$, and $e_i(t)$ is asymptotically close to $\frac{\chi_{ai} + \chi_{bi}}{2}$, where $\lim_{t \rightarrow \infty} \mathcal{A}_i(t) = \chi_{ai}$ and $\lim_{t \rightarrow \infty} \mathcal{B}_i(t) = \chi_{bi}$.

b) When achieving prescribed performance regulation, the mode vibration coordinates $q_i(t)$ of the flexible

link under input quantization converge to a small confined area around the origin, indicating the successful suppression of vibrations.

3 Preliminaries

3.1 Logarithmic quantization

The logarithmic quantizer $\mathcal{Q}(\cdot) : \mathbb{R} \rightarrow \mathcal{X}$ is employed to quantize the system’s inputs $\tau(t)$. With a quantization density parameter $0 < k < 1$, the logarithmic set of quantization levels is represented as $\mathcal{X} = \{\pm x_j : x_j = k^j x_0, j = 0, \pm 1, \pm 2, \dots\} \cup \{0\}$, where the initial value x_0 is a positive number.

The associated quantizer $\mathcal{Q}(\cdot)$ is defined as follows [35]:

$$\mathcal{Q}(\beta) = \begin{cases} x_i, & \text{if } \frac{1}{1+\delta}x_i < \beta \leq \frac{1}{1-\delta}x_i, \beta > 0; \\ 0, & \text{if } \beta = 0; \\ -\mathcal{Q}(-\beta), & \text{if } \beta < 0, \end{cases} \tag{8}$$

with the sector bound $\delta = \frac{1-k}{1+k} \in (0, 1)$.

3.2 Characteristic decomposition of logarithmic quantizer

In light of the approach proposed in [31], the logarithmic quantizer $\mathcal{Q}(\tau(t))$ can be constructed as below:

$$\mathcal{Q}(\tau(t)) = g_1(t)\tau(t) + g_2(t), \tag{9}$$

where two auxiliary parameters $g_j(t), j = 1, 2$ are defined as:

$$g_1(t) = \begin{cases} \frac{\mathcal{Q}(\tau(t))}{\tau(t)}, & \text{if } |\tau(t)| \geq b; \\ 1, & \text{if } |\tau(t)| < b; \end{cases} \tag{10}$$

$$g_2(t) = \begin{cases} 0, & \text{if } |\tau(t)| \geq b; \\ \mathcal{Q}(\tau(t)) - \tau(t), & \text{if } |\tau(t)| < b; \end{cases} \tag{11}$$

Note that the $g_1(t)$ is greater than zero in (10) during the quantitative process. If $|\tau(t)| \leq b$ with a positive input constraint $b > 0$, then $\mathcal{Q}(\tau(t))$ has bound, and thus $g_2(t)$ has upper bound limitation, that is $|g_2(t)| \leq \bar{g}_2$, where \bar{g}_2 is a positive constant.

3.3 Novel flexible prescribed performance statement

Definition 1 (Novel flexible prescribed performance \mathcal{X})

$$\mathcal{X} = \left\{ (t, e(t)) \in \mathbb{R}^+ \times \mathbb{R} \mid \mathcal{A}(t) < e(t) < \mathcal{B}(t), \lim_{t \rightarrow \infty} e(t) = \frac{\chi_a + \chi_b}{2} \right\}$$

where $\mathcal{A}(t)$ and $\mathcal{B}(t)$ are two smooth flexible prescribed performance functions that can be selected on the basis of actual circumstances, and the following requirements should be met in designing the flexible prescribed performance functions.

(i) Bounded property: $\mathcal{A}(t)$ and $\mathcal{B}(t)$ and their derivatives need to be bounded.

(ii) Limit condition: $\mathcal{A}(t)$ and $\mathcal{B}(t)$ exist limits such that $\lim_{t \rightarrow \infty} \mathcal{A}(t) = \chi_a$ and $\lim_{t \rightarrow \infty} \mathcal{B}(t) = \chi_b$.

(iii) Stability condition: $\mathcal{A}(t)$ and $\mathcal{B}(t)$ are chosen to meet that $\chi_a + \chi_b = 0$ (nonessential flexible condition).

Furthermore, in order to analyze the system stability, Lemma 1 is given on the property of parameter-type functions as follows:

Lemma 1 *The two parameter-type functions with respect to a function $\Pi(t)$ consist of the following:*

$$\mathcal{L}_1(\Pi(t)) = \ln \frac{\varpi}{\varpi - \Pi^2(t)}, \mathcal{L}_2(\Pi(t)) = \frac{\Pi^2(t)}{\varpi - \Pi^2(t)}, \tag{12}$$

where $\varpi \leq 1$ is a positive parameter. Then, the subsequent inequality is satisfied during the interval $-\sqrt{\varpi} < \Pi(t) < \sqrt{\varpi}$,

$$\mathcal{L}_1(\Pi(t)) \leq \mathcal{L}_2(\Pi(t)). \tag{13}$$

Proof By constructing $\mathcal{L}(\Pi(t)) = \mathcal{L}_2(\Pi(t)) - \mathcal{L}_1(\Pi(t))$, one has $\mathcal{L}(\Pi(t) = 0) = 0$, and differentiating $\mathcal{L}(\Pi(t))$ w.r.t. $\Pi(t)$ as follows:

$$\begin{aligned} \frac{d\mathcal{L}(\Pi(t))}{d\Pi(t)} &= \frac{d\mathcal{L}_2(\Pi(t))}{d\Pi(t)} - \frac{d\mathcal{L}_1(\Pi(t))}{d\Pi(t)} \\ &= \frac{2\Pi^3(t)}{(\varpi - \Pi^2(t))^2}, -\sqrt{\varpi} < \Pi(t) < \sqrt{\varpi}. \end{aligned} \tag{14}$$

In view of Eq. (14), one can derive $\frac{d\mathcal{L}(\Pi(t))}{d\Pi(t)} < 0$ among the interval $-\sqrt{\varpi} < \Pi(t) < 0$; it deduces that $\mathcal{L}(\Pi(t))$ can be monotonously reduced to zero, then $\mathcal{L}(\Pi(t)) > 0$ for $-\sqrt{\varpi} < \Pi(t) < 0$. Accordingly, $\mathcal{L}(\Pi(t)) > 0$ among the interval $\sqrt{\varpi} > \Pi(t) >$

0. Therefore, one can conclude that $\mathcal{L}(\Pi(t)) = \mathcal{L}_2(\Pi(t)) - \mathcal{L}_1(\Pi(t)) \geq 0$ for $-\sqrt{\varpi} < \Pi(t) < \sqrt{\varpi}$, which also indicates $\mathcal{L}_2(\Pi(t)) \geq \mathcal{L}_1(\Pi(t))$. \square

Remark 4 Different from the traditional prescribed performance design strategies [13,23–26], the developed FPPC scheme of this work has the following three merits.

(i) To improve both the dynamic and steady-state performance of regulation errors in the controlled robotic system, we introduce the parameter-type function $\Pi(t)$ by selecting appropriate prescribed performance functions. Additionally, it’s worth noting that from Eq. (12), it is evident that both of these performance aspects can also be adjusted by the parameter ϖ .

(ii) As for the prescribed performance functions $\mathcal{A}(t)$ and $\mathcal{B}(t)$, we proposed can be more flexible than other performance functions in [13,23–26], since they can be symmetrical or asymmetric.

(iii) Considering the global control strategy, the prescribed performance functions are generally chosen as the exponentially decaying function $v(t) = v_1 e^{-l_1 t} + v_\infty$ such that $\lim_{t \rightarrow \infty} v(t) = v_\infty$, and v_1, l_1 and v_∞ are normal constants. However, the v_∞ in our work can be set as $v_\infty \geq 0$.

4 Robust flexible prescribed performance controller design

The FPPC controller design with flexible prescribed performance tracking without and under input quantization is developed in this section, respectively. Both control goals of the above two considered cases are to realize $\theta(t)$ follow the desired joint angular positions $\theta_d(t)$ in an expected compact error set with suppressing the vibration of the flexible link around zero eventually.

4.1 Novel flexible prescribed performance without input quantization

The prescribed performance tracking control aims to create a satisfactory tracking performance of $x_1(t)$ following $x_{1d}(t)$. For the simplicity of the whole paper, the tracking error variables $e(t)$ as well as virtual error $z_2(t)$ are introduced as follows:

$$\begin{cases} e(t) = x_1(t) - x_{1d}(t) \\ z_2(t) = x_2(t) - \alpha(t) \end{cases} \tag{15}$$

where $\alpha(t)$ is a virtual control variable to be determined.

Step 1. Concerning the novel prescribed performance \mathcal{K} , the following Lyapunov function candidate is defined as:

$$V_1(t) = \sum_{j=1}^4 \ln \frac{\varpi_j}{\varpi_j - \Pi_j^2(t)}$$

with $\Pi_j(t) = \frac{e_j(t) - \mathcal{A}_j(t)}{\mathcal{B}_j(t) - \mathcal{A}_j(t)} + \frac{e_j(t) - \mathcal{B}_j(t)}{\mathcal{B}_j(t) - \mathcal{A}_j(t)}$. And its derivative w.r.t. time consists of the following:

$$\begin{aligned} dV_1(t)/dt &= \sum_{j=1}^4 \frac{2\Pi_j(t)}{(\mathcal{B}_j(t) - \mathcal{A}_j(t))(\varpi_j - \Pi_j^2(t))} \\ &\quad [2\dot{e}_j(t) - \dot{\mathcal{A}}_j(t) - \dot{\mathcal{B}}_j(t) - \Pi_j(t)(\dot{\mathcal{B}}_j(t) - \dot{\mathcal{A}}_j(t))] \\ &= \sum_{j=1}^4 \frac{2\Pi_j(t)}{(\mathcal{B}_j(t) - \mathcal{A}_j(t))(\varpi_j - \Pi_j^2(t))} \\ &\quad [2\dot{z}_{1j}(t) - \dot{\mathcal{A}}_j(t) - \dot{\mathcal{B}}_j(t) - \Pi_j(t)(\dot{\mathcal{B}}_j(t) - \dot{\mathcal{A}}_j(t))] \\ &= \sum_{j=1}^4 \frac{2\Pi_j(t)}{(\mathcal{B}_j(t) - \mathcal{A}_j(t))(\varpi - \Pi_j^2(t))} \\ &\quad [2(z_{2j}(t) + \alpha_j(t) - \dot{x}_{jd}(t)) - \dot{\mathcal{A}}_j(t) - \dot{\mathcal{B}}_j(t) \\ &\quad - \Pi_j(t)(\dot{\mathcal{B}}_j(t) - \dot{\mathcal{A}}_j(t))] \end{aligned} \tag{16}$$

Then, the virtual backstepping controller $\alpha_j(t)$ should be designed by:

$$\begin{aligned} \alpha_j(t) &= \dot{x}_{jd}(t) + \frac{1}{2}[\dot{\mathcal{A}}_j(t) + \dot{\mathcal{B}}_j(t) \\ &\quad + \Pi_j(t)(\dot{\mathcal{A}}_j(t) - \dot{\mathcal{B}}_j(t))] \\ &\quad - \frac{1}{2}k_1 \Pi_j(t)(\mathcal{B}_j(t) - \mathcal{A}_j(t)), \end{aligned} \tag{17}$$

Substituting $\alpha_j(t)$ into $\dot{V}_1(t)$, one gets:

$$\begin{aligned} \dot{V}_1(t) &= \sum_{j=1}^4 \frac{2\Pi_j(t)z_{2j}(t)}{(\mathcal{B}_j(t) - \mathcal{A}_j(t))(\varpi_j - \Pi_j^2(t))} \\ &\quad - \sum_{j=1}^4 \frac{k_1 \Pi_j^2(t)}{\varpi_j - \Pi_j^2(t)}, \end{aligned} \tag{18}$$

Step 2. To eliminate the term $z_{2j}(t)$ in Eq. (18), one can define:

$$V_2(t) = V_1(t) + \frac{1}{2}z_2^T(t)M(x_1(t))z_2(t). \tag{19}$$

Accordingly, the time derivative of $V_2(t)$ gives:

$$\begin{aligned} \dot{V}_2(t) &= \dot{V}_1(t) + \frac{1}{2}z_2^T(t)\dot{M}(x_1(t))z_2(t) \\ &\quad + z_2^T(t)M(x_1(t))\dot{z}_2(t) \\ &= \dot{V}_1(t) + \frac{1}{2}z_2^T(t)\dot{M}(x_1(t))(x_2(t) - \alpha(t)) \\ &\quad + z_2^T(t)M(x_1(t))(\dot{x}_2(t) - \dot{\alpha}(t)) \\ &= \dot{V}_1(t) + z_2^T(t) \left[M(x_1(t))(\dot{x}_2(t) - \dot{\alpha}(t)) \right. \\ &\quad \left. - \frac{1}{2}\dot{M}(x_1(t))\alpha(t) \right] \\ &\quad + \frac{1}{2}z_2^T(t)\dot{M}(x_1(t))x_2(t) \end{aligned} \tag{20}$$

With the equivalent formal (7), one can obtain

$$\begin{aligned} \dot{V}_2(t) &= \sum_{j=1}^4 \frac{2\Pi(t)z_{2j}(t)}{(\mathcal{B}_j(t) - \mathcal{A}_j(t))(\varpi_j - \Pi_j^2(t))} \\ &\quad - \sum_{j=1}^4 \frac{\Pi_j^2(t)}{\varpi_j - \Pi_j^2(t)} + \frac{1}{2}z_2^T(t)\dot{M}(x_1(t))x_2(t) \\ &\quad + z_2^T(t) \left[M(x_1(t))(\dot{x}_2(t) - \dot{\alpha}(t)) - \frac{1}{2}\dot{M}(x_1(t))\alpha(t) \right] \\ &= \sum_{j=1}^4 \frac{2\Pi(t)z_{2j}(t)}{(\mathcal{B}_j(t) - \mathcal{A}_j(t))(\varpi_j - \Pi_j^2(t))} \\ &\quad + z_2^T(t)[\tau(t) - Kx_1(t) - C(x_1, x_2)x_2(t) \\ &\quad - M(x_1)\dot{\alpha}(t) - \frac{1}{2}\dot{M}(x_1(t))\alpha(t)] \\ &\quad - \sum_{j=1}^4 \frac{k_1\Pi_j^2(t)}{\varpi_j - \Pi_j^2(t)} + \frac{1}{2}z_2^T(t)\dot{M}(x_1)x_2(t) \end{aligned} \tag{21}$$

Based on the property of inertia matrix [21], one gives that

$$C(x_1, x_2)x_2 = \dot{M}(x_1)x_2 - \frac{1}{2} \frac{\partial x_2^T(t)M(x_1)x_2(t)}{\partial x_1}$$

Then, one has

$$\begin{aligned} \dot{V}_2(t) &= \sum_{j=1}^4 \frac{2\Pi_j(t)z_{2j}(t)}{(\mathcal{B}_j(t) - \mathcal{A}_j(t))(\varpi_j - \Pi_j^2(t))} \\ &\quad + z_2^T(t)[\tau(t) - Kx_1(t) - M(x_1(t))\dot{\alpha}(t) \\ &\quad - \frac{1}{2}\dot{M}(x_1(t))\alpha(t)] - \sum_{j=1}^4 \frac{k_1\Pi_j^2(t)}{\varpi_j - \Pi_j^2(t)} \\ &= z_2^T(t)[\tau(t) - Kx_1(t) + 2\tilde{H}(t) - M(x_1(t))\dot{\alpha}(t) \\ &\quad - \frac{1}{2}\dot{M}(x_1(t))\alpha(t)] \\ &\quad - \sum_{j=1}^4 \frac{k_1\Pi_j^2(t)}{\varpi_j - \Pi_j^2(t)} \end{aligned} \tag{22}$$

with $\tilde{H}(t) \in \mathbb{R}^4$, $\tilde{H}_{j1}(t) = \frac{\Pi_j(t)}{(\mathcal{B}_j(t) - \mathcal{A}_j(t))(\varpi_j - \Pi_j^2(t))}$.

Step 3. Then, the FPPC tracking law is proposed as follows:

$$\begin{aligned} \tau(t) &= -k_2(x_2(t) - \alpha(t)) + Kx_1(t) + 0.5\dot{M}(x_1)\alpha(t) \\ &\quad - 2\tilde{H}(t) + M(x_1)\dot{\alpha}(t) \end{aligned} \tag{23}$$

In view of the above analysis, the achieved results without input quantization effect $\mathcal{Q}(\cdot)$ is summarized in Theorem 1.

Theorem 1 For the closed-loop RFCRSs (1), the FPPC control scheme (23) is proposed by adaptive backstepping approach to realize the prescribed tracking performance and vibration suppression such that:

- 1) $\lim_{t \rightarrow \infty} e_j(t) = \frac{(\chi_{aj} + \chi_{bj})}{2} = 0, j = 1, 2;$
- 2) $\lim_{t \rightarrow \infty} q_j(t) = \frac{(\chi_{aj} + \chi_{bj})}{2} = 0, j = 1, 2.$

Proof To better carry out the stable proof, an appropriate Lyapunov function is selected as follows:

$$V(t) = V_1(t) + \frac{1}{2}z_2^T(t)M(x_1(t))z_2(t). \tag{24}$$

With the previous analysis (22), then substituting the above FPPC law (23) into Eq. (19), one has

$$\begin{aligned} \dot{V}(t) &= -k_1 \sum_{j=1}^4 \frac{\Pi_j^2(t)}{\varpi_j - \Pi_j^2(t)} - k_2 z_2^T(t)z_2(t) \\ &= -k_1 \sum_{j=1}^4 \ln \frac{\varpi_j}{\varpi_j - \Pi_j^2(t)} - k_2 z_2^T(t)z_2(t) \\ &\leq -c_1 V(t) \end{aligned} \tag{25}$$

with $c_1 = \min\{k_1, \frac{2k_2}{\lambda_{\max}(M(x_1))}\}$. □

According to Ineq. (25), the two conclusions can be made in the following propositions:

Property 1 According to Ineq. (25) and Barbalat’s Lemma, one can derive

$$\lim_{t \rightarrow \infty} \ln \frac{\varpi_j}{\varpi_j - \Pi_j^2(t)} = 0. \tag{26}$$

Since $\Pi_j(t) = \frac{e_j(t) - \mathcal{A}_j(t)}{\mathcal{B}_j(t) - \mathcal{A}_j(t)} + \frac{e_j(t) - \mathcal{B}_j(t)}{\mathcal{B}_j(t) - \mathcal{A}_j(t)}$, it follows that

$$\begin{aligned} \lim_{t \rightarrow \infty} \Pi_j(t) = 0 &\Rightarrow \lim_{t \rightarrow \infty} \left\{ \frac{e_j(t) - \mathcal{A}_j(t)}{\mathcal{B}_j(t) - \mathcal{A}_j(t)} + \frac{e_j(t) - \mathcal{B}_j(t)}{\mathcal{B}_j(t) - \mathcal{A}_j(t)} \right\} = 0 \\ &\Rightarrow \lim_{t \rightarrow \infty} 2e_j(t) = \lim_{t \rightarrow \infty} (\mathcal{A}_j(t) + \mathcal{B}_j(t)) \\ &\Rightarrow \lim_{t \rightarrow \infty} e_j(t) = \lim_{t \rightarrow \infty} \frac{1}{2}(\mathcal{A}_j(t) + \mathcal{B}_j(t)) \end{aligned}$$

Property 2 By virtue of Ineq. (25), one gives

$$\begin{aligned} &\Rightarrow \dot{V}(t) \leq -c_1 V(t) \\ &\Rightarrow -\sqrt{\varpi_j - \varpi_j e^{-V(0)e^{-c_1 t}}} \leq \Pi_j(t) \\ &\leq \sqrt{\varpi_j - \varpi_j e^{-V(0)e^{-c_1 t}}} \\ &\Rightarrow -1 \leq -\sqrt{\varpi_j} < \frac{2e_j(t) - \mathcal{A}_j(t) - \mathcal{B}_j(t)}{\mathcal{B}_j(t) - \mathcal{A}_j(t)} \\ &< \sqrt{\varpi_j} \leq 1 \\ &\Rightarrow \mathcal{A}_j(t) < e_j(t) < \mathcal{B}_j(t), j = 1, 2. \end{aligned} \tag{27}$$

The above two properties deduce that this proposed method not only has the prescribed performance $\mathcal{A}_j(t) < e_j(t) < \mathcal{B}_j(t)$ but also can guarantee the limits of tracking errors meet that $\lim_{t \rightarrow \infty} e_j(t) = \lim_{t \rightarrow \infty} \frac{1}{2}(\mathcal{A}_j(t) + \mathcal{B}_j(t)) = \frac{1}{2}(\chi_{aj} + \chi_{bj}) = 0$ with $j = 1, 2$. Accordingly, the mode vibration suppression can be realized such that $\lim_{t \rightarrow \infty} q_j(t) = \frac{\chi_{aj} + \chi_{bj}}{2} = 0$.

Theorem 1 has now been fully demonstrated.

Remark 5 In the context of measuring flexible vibration deformation, the utilization of two strain gauge sensors is employed (the quantity of sensors being determined by the truncation order). In the case of the first two vibration modes, namely $q_1(t)$ and $q_2(t)$, the specific approach involves affixing a strain gauge to the flexible arm. As the flexible arm undergoes movement within the system, it induces vibrations and deformations across a broad range of motion. Consequently, the strain gauge generates strain as a result. The ensuing analog voltage signal is acquired through the half-bridge method within a bridge box. Subsequently, the signal undergoes filtering and amplification via dynamic strain gauge equipment. The primary purpose of the strain gauge is to measure the bending deformation of the flexible arm.

Remark 6 In relation to the feasibility of implementing the proposed method in real-time, employing robust adaptive FPPC laws, it is evident that the controllers only require information about $\theta(t)$ and $\dot{\theta}(t)$, both of which can be measured using a photoelectric encoder and tachometer, respectively. However, it's important to acknowledge that it's practically impossible to entirely eliminate the influence of sensor noise, which can affect the implementation of control, especially when dealing with time-differentiating terms. The encoder and strain gauge sensor are capable of detecting the rotation

angle $\theta(t)$ and deflection, providing real-time graphical data representation. To compute the signal derivatives for angular displacement $\theta(t)$, a derivative filter is employed. For real-time experiments, the MATLAB Simulink module generates control input signals, and the associated control performance can be visualized on an oscillograph.

4.2 Quantized flexible prescribed performance control design

In light of the dynamic equations and the control objective, the appropriate logarithmic quantizer is utilized to quantize control signals. The quantized control law and parameter update law are developed to track the desired joint angular positions and to guarantee the controlled RFCRSs are stable. The control block of the above quantized FPPC scheme is depicted in Fig. 2.

Following are the two portions of the primary quantized control input:

$$\begin{cases} \mathcal{Q}(\tau_i(t)) = g_{i1}(t)\tau_i(t) + g_{i2}(t) \\ \tau_i(t) = \frac{(x_{2i}(t) - \alpha_i(t))\hat{\mu}_i^2(t)\bar{\tau}_i^2(t)}{|(x_{2i}(t) - \alpha_i(t))\hat{\mu}_i(t)\bar{\tau}_i(t)| + \rho_i}, i = 1, 2 \end{cases} \tag{28}$$

where ρ_i is a normal constant and $\mu_i(t) = \frac{1}{\inf g_{li}(t)}$.

Two adaptive laws $\hat{\mu}(t)$ are expressed as:

$$\dot{\hat{\mu}}_j(t) = \gamma_j z_{2j}(t)\bar{\tau}_j(t) - \gamma_j \sigma_j \hat{\mu}_j(t), \quad j = 1, 2. \tag{29}$$

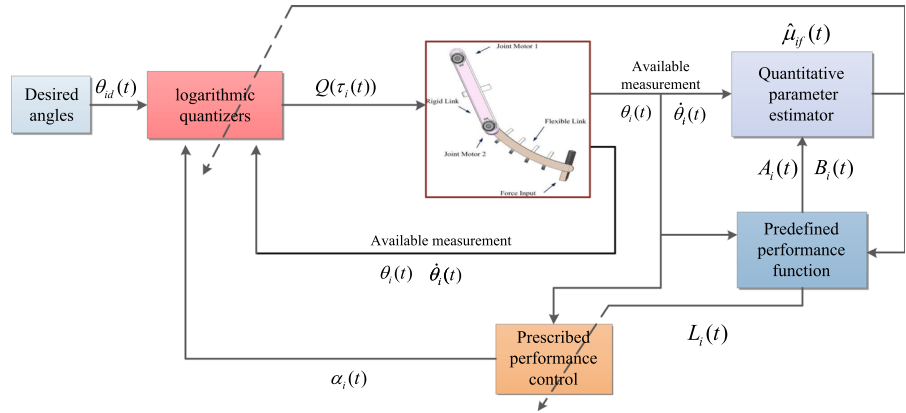
with two positive control gains γ_j, σ_j .

The auxiliary control $\bar{\tau}(t) \in \mathbb{R}^4$ and virtual backstepping controller $\alpha_i(t) \in \mathbb{R}$ are proposed as below:

$$\begin{aligned} \bar{\tau}(t) &= -k_2(x_2(t) - \alpha(t)) + Kx_1(t) + 0.5\dot{M}(x_1)\alpha(t) \\ &\quad + 2\tilde{H}(t) + M(x_1(t))\dot{\alpha}(t). \tag{30} \\ \alpha_j(t) &= \dot{x}_{jd}(t) + \frac{1}{2}[\dot{\mathcal{A}}_j(t) + \dot{\mathcal{B}}_j(t) \\ &\quad + \Pi_j(t)(\dot{\mathcal{A}}_j(t) - \dot{\mathcal{B}}_j(t))] \\ &\quad - \frac{1}{2}k_1\Pi_j(t)(\mathcal{B}_j(t) - \mathcal{A}_j(t)), j = 1, 2. \\ \tau(t) &= [I_2 \quad 0]^T \bar{\tau}(t) \end{aligned} \tag{31}$$

with $\Pi_j(t) = \frac{e_j(t) - \mathcal{A}_j(t)}{\mathcal{B}_j(t) - \mathcal{A}_j(t)} + \frac{e_j(t) - \mathcal{B}_j(t)}{\mathcal{B}_j(t) - \mathcal{A}_j(t)}$.

Fig. 2 The quantized control block of the RFCRSs with flexible prescribed performance



5 Stability analysis of the controlled RFCRSs

In this section, the main results of the flexible prescribed performance control with input quantization are demonstrated in the subsequent Theorem 2.

Theorem 2 According to the reduced dynamics of the RFCRSs described by (7), with the quantized FPCC control law (28) and the adaptation law (29), the tracking errors of the controlled RFCRSs under the prescribed performance are guaranteed. Error signals, $z_2(t)$ and $\tilde{\mu}(t)$ will remain within the compact sets Ω_{z_2} , $\Omega_{\tilde{\mu}}$, respectively, defined as follows:

$$\Omega_{z_2} := \left\{ z_2(t) \in \mathbb{R}^4 \mid \|z_2(t)\| \leq \sqrt{\frac{D}{\lambda_{\min}(M)}} \right\} \quad (32)$$

$$\Omega_{\tilde{\mu}} := \left\{ \tilde{\mu}(t) \in \mathbb{R}^2 \mid \|\tilde{\mu}(t)\| \leq \sqrt{\gamma \mu D} \right\} \quad (33)$$

where $D = 2(V(0) + \lambda/c_2)$ with two positive constants c_2 and λ , and $\gamma = \max\{\gamma_1, \gamma_2\}$ as well as $\mu = \max\{\mu_1, \mu_2\}$.

Proof In order to eliminate the input quantization influence, the control gains $g_{1i}(t)$ need to be estimated and the adaptive parameter law $\hat{\mu}_i(t)$ is introduced to observe the low bound value $\mu_i(t) = \frac{1}{\inf\{g_{1i}(t)\}}$, the following Lyapunov function candidate is defined as follows:

$$V(t) = \sum_{i=1}^2 \ln \frac{\varpi_i}{\varpi_i - \Pi_i^2(t)} + \sum_{i=1}^2 \frac{1}{2\gamma_i \mu_i} \tilde{\mu}_i^2(t) + \frac{1}{2} z_2^T(t) M(x_1(t)) z_2(t) \quad (34)$$

where $\gamma_i > 0, i = 1, 2$ is positive constants and $\tilde{\mu}(t) = \bar{\mu}(t) - \mu(t)$.

Because $g_1(t) > 0$, we know $\mu(t) > 0$. With the definition of $\bar{\mu}(t)$, the derivative of $V(t)$ is:

$$\begin{aligned} \dot{V}(t) &= z_2^T(t) [Q(\tau(t)) - Kx_1(t) + 2\tilde{H}(t) - M(x_1(t))\dot{\alpha}(t)] \\ &\quad - \frac{1}{2} \dot{M}(x_1(t))\alpha(t) \\ &\quad + \sum_{i=1}^2 \frac{1}{\gamma_i \mu_i(t)} \tilde{\mu}_i(t) \dot{\mu}_i(t) - \sum_{i=1}^2 \frac{k_1 \Pi_i^2(t)}{\varpi_i - \Pi_i^2(t)} \\ &= \sum_{i=1}^2 z_{2i}(t) [g_{1i}(t)\tau_i(t) + g_{2i}(t)] + z_2^T(t) [2\tilde{H}(t) \\ &\quad - Kx_1(t) - M(x_1(t))\dot{\alpha}(t)] \\ &\quad - \frac{1}{2} \dot{M}(x_1(t))\alpha(t) + \sum_{i=1}^2 \frac{1}{\gamma_i \mu_i(t)} \tilde{\mu}_i(t) \dot{\mu}_i(t) \\ &\quad - \sum_{i=1}^2 \frac{k_1 \Pi_i^2(t)}{\varpi_i - \Pi_i^2(t)} \end{aligned} \quad (35)$$

With the analysis of logarithmic quantizer (9), one obtains

$$\begin{aligned} \dot{V}(t) &= \sum_{i=1}^2 z_{2i}(t) [g_{1i}(t)\tau_i(t) + g_{2i}(t)] + z_2^T(t) \\ &\quad [-k_2 z_2(t) + k_2 z_2(t) - Kx_1(t) + 2\tilde{H}(t) \\ &\quad - M(x_1(t))\dot{\alpha}(t)] - \frac{1}{2} \dot{M}(x_1(t))\alpha(t) \\ &\quad + \sum_{i=1}^2 \frac{1}{\gamma_i \mu_i(t)} \tilde{\mu}_i(t) \dot{\mu}_i(t) - \sum_{i=1}^2 \frac{k_1 \Pi_i^2(t)}{\varpi_i - \Pi_i^2(t)} \\ &= \sum_{i=1}^2 z_{2i}(t) [g_{1i}(t)\tau_i(t) + g_{2i}(t)] - k_2 z_2^T(t) z_2(t) \\ &\quad + z_2^T(t) \bar{\tau}(t) - \sum_{i=1}^2 \frac{k_1 \Pi_i^2(t)}{\varpi_i - \Pi_i^2(t)} \\ &\quad + \sum_{i=1}^2 \frac{1}{\gamma_i \mu_i(t)} \tilde{\mu}_i(t) [\gamma_i z_{2i}(t) \bar{\tau}_i(t) - \gamma_i \sigma_i \hat{\mu}_i(t)] \end{aligned}$$

$$\begin{aligned} &\leq -k_2 z_2^T(t) z_2(t) + \sum_{i=1}^2 z_{2i}(t) g_{1i}(t) \tau_i(t) \\ &\quad + \sum_{i=1}^2 \frac{1}{\mu_i(t)} \tilde{\mu}_i(t) [z_{2i}(t) \bar{\tau}_i(t) - \sigma_i \hat{\mu}_i(t)] \\ &\quad - \sum_{i=1}^2 \left[\frac{k_1 \Pi_i^2(t)}{\varpi_i - \Pi_i^2(t)} + z_{2i}(t) \bar{g}_{2i}(t) \right] \\ &\quad + \sum_{i=1}^4 z_{2i}(t) \bar{\tau}_i(t) \end{aligned}$$

Substituting Eqs. (29)–(30) into the above inequality, one has

$$\begin{aligned} \dot{V}(t) &\leq -k_2 z_2^T(t) z_2(t) - \sum_{i=1}^2 \frac{k_1 \Pi_i^2(t)}{\varpi_i - \Pi_i^2(t)} \\ &\quad - \sum_{i=1}^2 z_{2i}(t) g_{1i}(t) \frac{(x_{2i}(t) - \alpha_i(t)) \hat{\mu}_i^2(t) \bar{\tau}_i^2(t)}{|(x_{2i}(t) - \alpha(t)) \hat{\mu}(t) \bar{\tau}(t)| + \rho_i} \\ &\quad + \sum_{i=1}^2 \frac{1}{\mu_i(t)} \tilde{\mu}_i(t) [z_{2i}(t) \bar{\tau}_i(t) - \sigma_i \hat{\mu}_i(t)] \\ &\quad + \sum_{i=1}^2 z_{2i}(t) \bar{g}_{2i}(t) + \sum_{i=1}^4 z_{2i}(t) \bar{\tau}_i(t) \\ &\leq -k_2 z_2^T(t) z_2(t) - \sum_{i=1}^2 \frac{k_1 \Pi_i^2(t)}{\varpi_i - \Pi_i^2(t)} \\ &\quad + \sum_{i=1}^2 z_{2i}(t) \bar{g}_{2i}(t) + \sum_{i=1}^4 z_{2i}(t) \bar{\tau}_i(t) \\ &\quad + \sum_{i=1}^2 \frac{1}{\mu_i(t)} \tilde{\mu}_i(t) [z_{2i}(t) \bar{\tau}_i(t) - \sigma_i \hat{\mu}_i(t)] \\ &\quad - \sum_{i=1}^2 g_{1i}(t) \frac{z_{2i}^2(t) \hat{\mu}_i^2(t) \bar{\tau}_i^2(t)}{|z_{2i}(t) \hat{\mu}_i(t) \bar{\tau}_i(t)| + \rho_i} \end{aligned} \tag{36}$$

Since

$$|\xi| - \frac{|\xi|^2}{\rho_i + |\xi|} = \frac{\rho_i |\xi|}{\rho_i + |\xi|} < \rho_i \tag{37}$$

Then

$$-\frac{z_{2i}^2(t) \hat{\mu}_i^2(t) \bar{\tau}_i^2(t)}{|z_{2i}(t) \hat{\mu}_i(t) \bar{\tau}_i(t)| + \rho_i} < \rho_i - z_{2i}(t) \hat{\mu}_i(t) \bar{\tau}_i(t) \tag{38}$$

Noticing that $g_{1i}(t) \geq g_{1imin} = \frac{1}{\mu_i(t)} > 0$, one gets

$$-g_{1i} \frac{z_{2i}^2(t) \hat{\mu}_i^2(t) \bar{\tau}_i^2(t)}{|z_{2i}(t) \hat{\mu}_i(t) \bar{\tau}_i(t)| + \rho_i} < \frac{1}{\mu_i} (\rho_i - z_{2i}(t) \hat{\mu}_i(t) \bar{\tau}_i(t)) \tag{39}$$

With the above relationship (39), one has

$$\begin{aligned} \dot{V}(t) &\leq -(k_2 - 1) z_2^T(t) z_2(t) + \sum_{i=1}^4 z_{2i}(t) \bar{\tau}_i(t) + \bar{g}_2^2(t) \\ &\quad + \sum_{i=1}^2 \frac{1}{\mu_i} \rho_i \\ &\quad + \sum_{i=1}^2 \frac{1}{\mu_i(t)} [\tilde{\mu}_i(t) z_{2i}(t) \bar{\tau}_i(t) - z_{2i}(t) \hat{\mu}_i(t) \bar{\tau}_i(t)] \\ &\quad - \sum_{i=1}^2 \left[\frac{k_1 \Pi_i^2(t)}{\varpi_i - \Pi_i^2(t)} + \frac{1}{\mu_i(t)} \tilde{\mu}_i(t) \sigma_i \hat{\mu}_i(t) \right] \\ &\leq -(k_2 - 1) z_2^T(t) z_2(t) + \sum_{i=3}^4 z_{2i}(t) \bar{\tau}_i(t) \\ &\quad - \sum_{i=1}^2 \frac{k_1 \Pi_i^2(t)}{\varpi_i - \Pi_i^2(t)} \\ &\quad - \sum_{i=1}^2 \frac{1}{\mu_i(t)} \tilde{\mu}_i(t) \sigma_i \hat{\mu}_i(t) + \bar{g}_2^2(t) + \sum_{i=1}^2 \frac{1}{\mu_i} \rho_i \end{aligned} \tag{40}$$

with $\bar{g}_2^2(t) = \max\{\bar{g}_{21}(t), \bar{g}_{22}(t)\}$. □

Since the RFCRSs only has two real input $\tau_j(t)$ with $j = 1, 2$, and $\bar{\tau}_j(t)$ with $j = 3, 4$ in Eq. (30) is not required, there exists two extra virtual controller $\alpha_j(t)$ with $j = 3, 4$ such that

$$\sum_{i=3}^4 z_{2i}(t) \bar{\tau}_i(t) = 0. \tag{41}$$

With the above relation, one can obtain

$$\begin{aligned} \dot{V}(t) &\leq -(k_2 - 1) z_2^T(t) z_2(t) - \sum_{i=1}^2 \frac{k_1 \Pi_i^2(t)}{\varpi_i - \Pi_i^2(t)} + \bar{g}_2^2(t) \\ &\quad - \sum_{i=1}^2 \frac{1}{\mu_i(t)} \tilde{\mu}_i(t) \sigma_i \hat{\mu}_i(t) + \sum_{i=1}^2 \frac{1}{\mu_i} \rho_i \end{aligned} \tag{42}$$

Noticing that

$$\begin{aligned} -\tilde{\mu}_i(t) \hat{\mu}_i(t) &= -\tilde{\mu}_i(t) (\tilde{\mu}_i(t) + \mu_i) = -\tilde{\mu}_i^2(t) - \tilde{\mu}_i(t) \mu_i \\ &\leq -\tilde{\mu}_i^2(t) + \frac{1}{2} \tilde{\mu}_i^2(t) + \frac{1}{2} \mu_i^2(t) = -\frac{1}{2} \tilde{\mu}_i^2(t) + \frac{1}{2} \mu_i^2(t) \end{aligned} \tag{43}$$

Then,

$$-\frac{1}{\mu_i} \tilde{\mu}_i(t) \sigma_i \hat{\mu}_i(t) \leq -\frac{\sigma_i}{2} \tilde{\mu}_i^2(t) + \frac{\sigma_i}{2} \mu_i^2(t) \tag{44}$$

Therefore, one has

$$\begin{aligned} \dot{V}(t) \leq & -(k_2 - 1)z_2^T(t)z_2(t) - \sum_{i=1}^2 \frac{k_1 \Pi_i^2(t)}{\varpi_i - \Pi_i^2(t)} + \bar{g}_2^2(t) \\ & - \sum_{i=1}^2 \frac{\sigma_1}{2} \tilde{\mu}_i^2(t) + \sum_{i=1}^2 \frac{\sigma_i}{2} \mu_i^2(t) + \sum_{i=1}^2 \frac{1}{\mu_i} \rho_i \end{aligned} \quad (45)$$

By using Lemma 1, one can obtain

$$\begin{aligned} \dot{V}(t) \leq & -(k_2 - 1)z_2^T(t)z_2(t) - k_1 \sum_{i=1}^2 \ln \frac{\varpi_i}{\varpi_i - \Pi_i^2(t)} \\ & - \sum_{i=1}^2 \frac{\sigma_1}{2} \tilde{\mu}_i^2(t) + \sum_{i=1}^2 \frac{\sigma_i}{2} \mu_i^2(t) \\ & + \sum_{i=1}^2 \frac{1}{\mu_i} \rho_i + \bar{g}_2^2(t) \\ \leq & -c_2 V(t) + \lambda \end{aligned} \quad (46)$$

with $c_2 = \min\{\gamma_1 \sigma, 2k_1, \frac{2(k_2-1)}{\lambda_{\max}(M(x_1))}\}$ and $\lambda = \bar{g}_2(t) + \sum_{i=1}^2 \frac{\sigma_i}{2} \mu_i^2(t) + \sum_{i=1}^2 \frac{1}{\mu_i} \rho_i$.

Then, one can derive that

$$V(t) \leq \frac{\lambda}{c_2} + \left(V(0) - \frac{\lambda}{c_2} \right) e^{-c_2 t} \leq \frac{\lambda}{c_2} + V(0) \quad (47)$$

Meanwhile, one has

$$\frac{1}{2} \|z_2(t)\|^2 \leq \left(\frac{\lambda}{c_2} + V(0) \right) / \lambda_{\min}(M), \quad (48)$$

$$\frac{1}{2\gamma\mu} \|\tilde{\mu}(t)\|^2 \leq \frac{\lambda}{c_2} + V(0) \quad (49)$$

with $\gamma = \max\{\gamma_1, \gamma_2\}$ and $\mu = \max\{\mu_1, \mu_2\}$.

It can be seen from Ineq. (47) that $\sqrt{\ln \frac{\varpi_i}{\varpi_i - \Pi_i^2(t)}}$ is uniformly ultimately converge to a bounded compact set \mathcal{E} . Given any $\varsigma_*^2 > \frac{2\lambda}{c_2} > 0$, then it selects T meets that $\ln \frac{\varpi_i}{\varpi_i - \Pi_i^2(t)} \leq \varsigma_*^2, |z_i(t)| \leq \varsigma_*^2, \forall t > T$.

Thus, the compact set \mathcal{E} can be defined as $\{z_i \in \mathbb{R}^4 : \ln \frac{\varpi_i}{\varpi_i - \Pi_i^2(t)} \leq \varsigma_*^2, |z_i(t)| \leq \varsigma_*^2\}$

In terms of the aforesaid observation, it follows that $\ln \frac{\varpi_i}{\varpi_i - \Pi_i^2(t)} \leq \varsigma_*^2$ and further derived as follows:

$$\begin{aligned} \ln \frac{\varpi_i}{\varpi_i - \Pi_i^2(t)} \leq \varsigma_*^2 & \Rightarrow -\sqrt{\varpi_i e^{-\varsigma_*^2}} \leq \Pi_i(t) \leq \sqrt{\varpi_i e^{-\varsigma_*^2}} \\ \Rightarrow e_i(t) \leq & \frac{\mathcal{B}_i + \mathcal{A}_i + (\mathcal{B}_i - \mathcal{A}_i)\sqrt{\varpi_i e^{-\varsigma_*^2}}}{2} \end{aligned} \quad (50)$$

Further, there selects μ^* sufficiently small via adjusting the parameters, then tracking errors $e_i(t)$ approach $(\chi_{ai} + \chi_{bi})/2$ with $i = 1, 2$.

With the definition of $\Pi_i(t)$, one can derive

$$\begin{aligned} \sqrt{\varpi_i e^{-\varsigma_*^2}} \leq \sqrt{\varpi_i} < 1 & \Rightarrow (\mathcal{B}_i - \mathcal{A}_i)\sqrt{\varpi_i e^{-\varsigma_*^2}} < \mathcal{B}_i - \mathcal{A}_i \\ \Rightarrow \frac{\mathcal{B}_i + \mathcal{A}_i + (\mathcal{B}_i - \mathcal{A}_i)\sqrt{\varpi_i e^{-\varsigma_*^2}}}{2} & < \mathcal{B}_i \end{aligned} \quad (51)$$

Similarly, one can also derive that

$$\frac{\mathcal{B}_i + \mathcal{A}_i - (\mathcal{B}_i - \mathcal{A}_i)\sqrt{\varpi_i e^{-\varsigma_*^2}}}{2} > \mathcal{A}_i \quad (52)$$

Combining Ineq. (50) with Ineqs. (51)–(52), one has

$$\mathcal{A}_i(t) < e_i(t) < \mathcal{B}_i(t) \quad \text{with } i = 1, 2. \quad (53)$$

It should be concluded from the above analysis that the tracking errors of angular position $e_i(t)$ are constrained between \mathcal{A}_i and \mathcal{B}_i by virtue of selecting appropriate functions \mathcal{A}_i and \mathcal{B}_i , which also indicates that RFCRSs achieve prescribed performance \mathcal{K} defined in Definition 1.

This is the end of Theorem 2.

6 Numerical simulation

To demonstrate the viability of the constructed control law with flexible prescribed regulation performance. These simulation results on the comparison with the PD law [39], different flexible functions, and logarithmic quantization will be divided into three cases to demonstrate.

Simulation of flexible prescribed performance control will be shown in the first part. A PD controller [39] will be introduced in the second part in comparison. Both the PD controller and the prescribed performance controller based on the logarithm quantizer will be revealed in the third part. The parameters of rigid–flexible robotic systems are specified in Table 1. The desired angular positions are chosen as $\theta_{1d} = 0.5, \theta_{2d} = 0.8$.

Case 1. Novel flexible prescribed performance control without quantization in comparison with PD control

Regarding this PD control law [39] is utilized to achieve the tracking control of angular position and the flexible link’s ability to reduce vibration in comparison with the proposed FPPC laws. The PD control is described by: $u_j(t) = -k_{jp}(\theta_j(t) - \theta_{jd}) - k_{jd}\dot{\theta}_j(t)$, where k_{jp} and k_{jd} are positive gains with $j = 1, 2$.

The corresponding control values and performance functions are listed as follows: $k_{1p} = 38, k_{1d} = 22, k_{2p} = 23, k_{2d} = 5$;

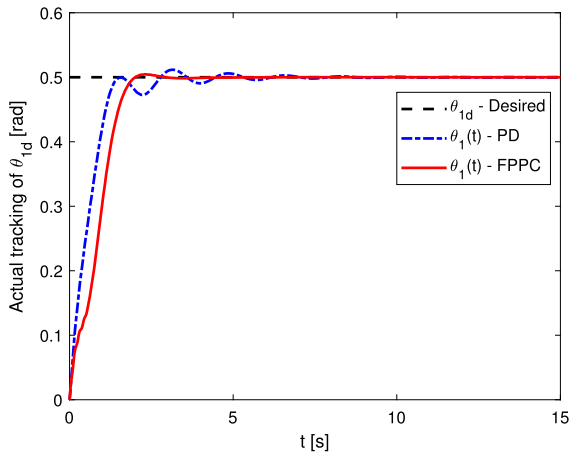


Fig. 3 Actual tracking of θ_{1d} (rad) in Case 1

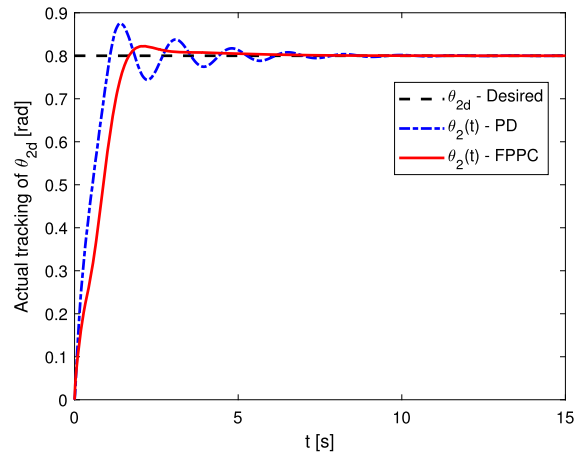


Fig. 4 Actual tracking of θ_{2d} (rad) in Case 1

$k_1 = 1.8, k_2 = 3.6, \mathcal{A}_1(t) = -0.65$ and $\mathcal{B}_1(t) = 0.65 + 0.7e^{-8t}, \mathcal{A}_2(t) = -0.50 - e^{-1t}, \mathcal{B}_2(t) = 0.50 + 0.6e^{-0.72t}$.

The real profiles of two angular position regulation using PD and FPPC control are depicted in Figs. 3, 4, respectively. It is clear that the advocated FPPC method provides superior regulation performance than the comparative PD control [39], especially as can be seen from the small windows of Figs. 3 and 4. To show the deformation of flexible beam, the flexible displacements of general 1st and 2nd mode coordinates are shown in Figs. 5, 6. In view of the above vibrations in Figs. 5, 6, the vibration of the flexible beam is quickly eliminated approach zero, and the suppression effect of the developed FPPC law is faster than the compared PD control. It is noted that the first mode vibration is the dominant frequency and the second mode will also be suppressed as the first mode vibration reduces to zero in Figs. 5, 6. The corresponding vibration surface using the PD law and FPPC laws are revealed in Figs. 7, 8. Although the reduced rigid–flexible robotic system has high mode numbers, the regulation control performance is not influenced as shown in Figs. 9, 10. It can also be observed that the two-mode vibrations can be suppressed rapidly and smoothly with the proposed method in comparison with the PD control law [39].

In view of the above comparison simulations, although the traditional PD control [39] has a positive effect on trajectory regulation and vibration suppression, its control performance is not satisfactory in comparison with the developed robust adaptive FPPC method.

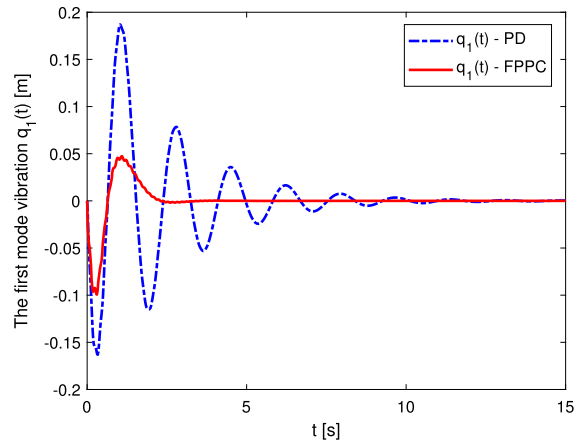


Fig. 5 1st mode vibration $q_1(t)$ (m) in Case 1

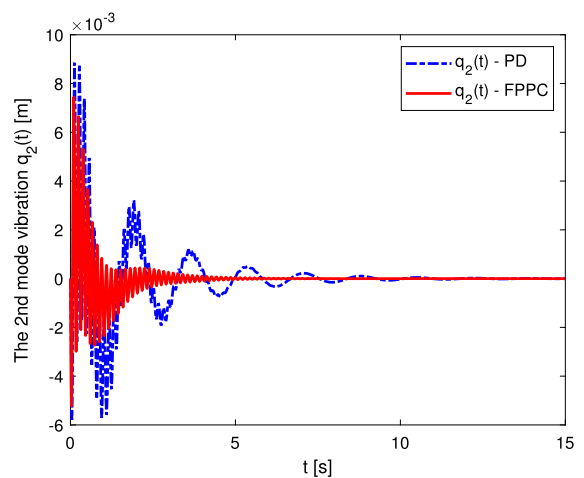


Fig. 6 2nd mode vibration $q_2(t)$ (m) in Case 1

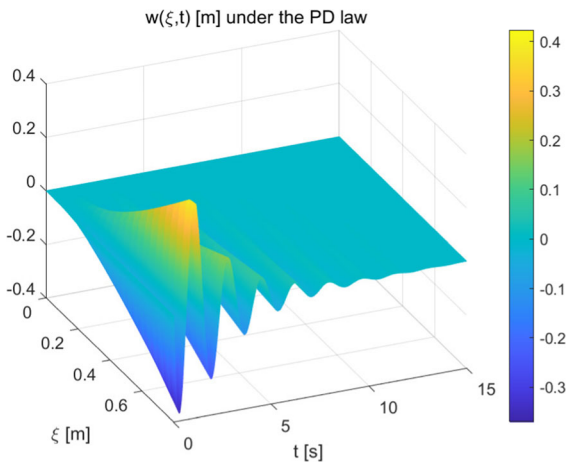


Fig. 7 The total vibration surface $w(\xi, t)$ (m) under the PD law

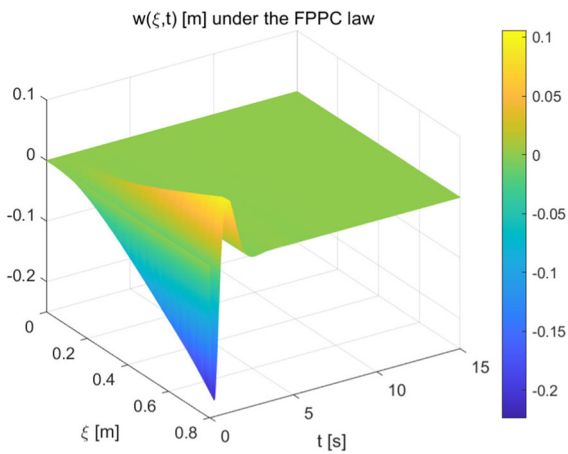


Fig. 8 The total vibration surface $w(\xi, t)$ (m) under the FPPC law

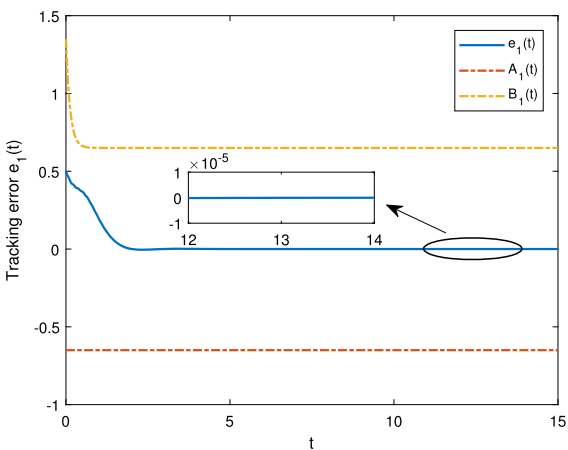


Fig. 9 Regulation index $e_1(t)$ (rad) under FPPC law in Case 1

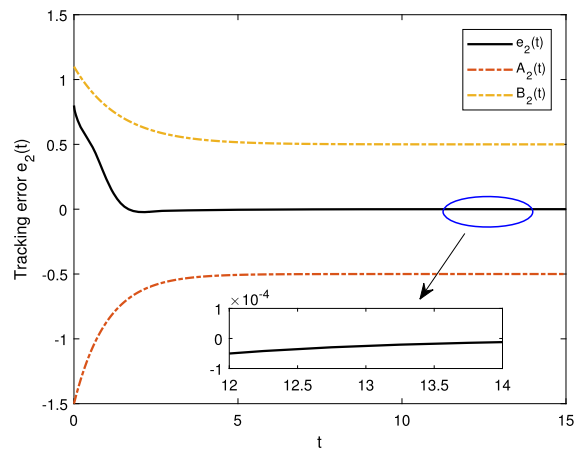


Fig. 10 Regulation index $e_2(t)$ (rad) under FPPC law in Case 1

The control gains for the quantized FPPC scheme are determined through the following procedures:

1. Setting the quantized parameters as $\rho_1 = \rho_2 = 0.01$ and $k_1 = k_2 = 0.01$. Then, increment the value of K from zero until the controlled system exhibits slight oscillations to some extent.
2. Determining the maximum error and error rate of the two angular positions under the tuned values of k_1 and k_2 . Initially, choose half of the maximum error as the value for k_1 and half of the maximum error rate as k_2 . Subsequently, increase the values of $\rho_j, j = 1, 2$ while simultaneously decreasing the value of K to further minimize the error, making necessary trade-offs between the two parameters.
3. Maintaining the tuning of $k_j, j = 1, 2$ and K achieved in the first two stages, and then increase the values of σ_j and $\gamma_j, j = 1, 2$ to enhance dynamic regulation and vibration suppression performance. Next, finely adjust these two values and strike a balance between σ_j and γ_j .

Case 2. Novel flexible prescribed performance with different functional sets \mathcal{K}

To better present the flexible prescribed performance under the limitations on a functional set \mathcal{K} . Some feature prescribed functions with different converge speeds are taken and the following three comparison conditions are considered:

Condition 1) $\mathcal{A}_{11}(t) = -0.58, \mathcal{B}_{11}(t) = 0.58 + 0.3e^{-8t}$, and $\mathcal{A}_{12}(t) = -0.5 - 0.5e^{-0.75t}, \mathcal{B}_{12}(t) = 0.5 + 0.6e^{-0.8t}$;

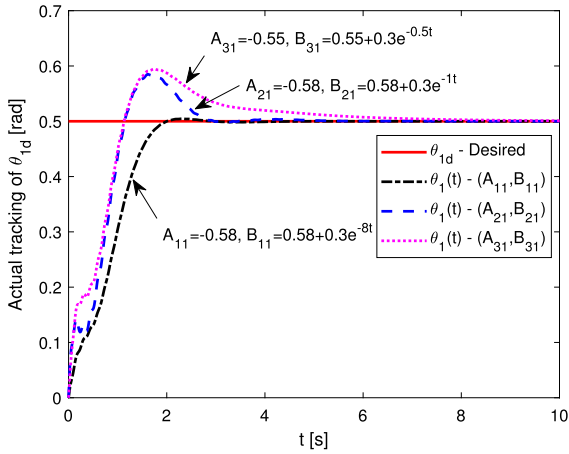


Fig. 11 Actual tracking of θ_{1d} (rad) with different FPPCs in Case 2

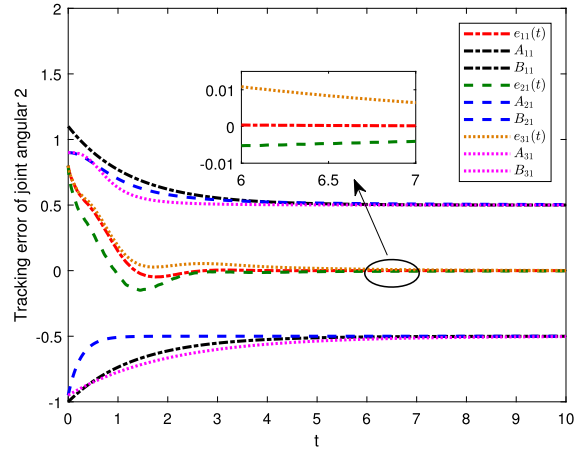


Fig. 14 Regulation index $e_2(t)$ (rad)—Case 2

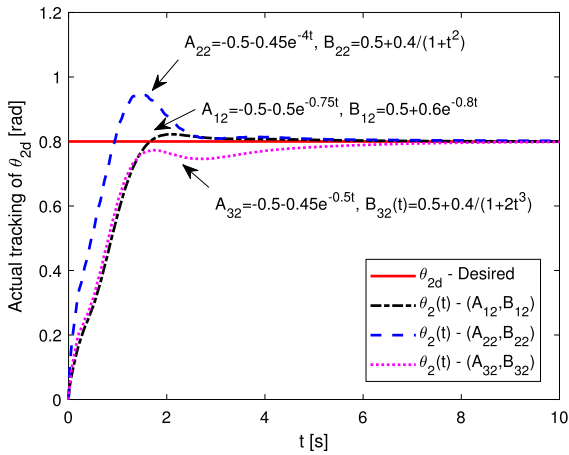


Fig. 12 Actual tracking of θ_{2d} (rad) with different FPPCs in Case 2

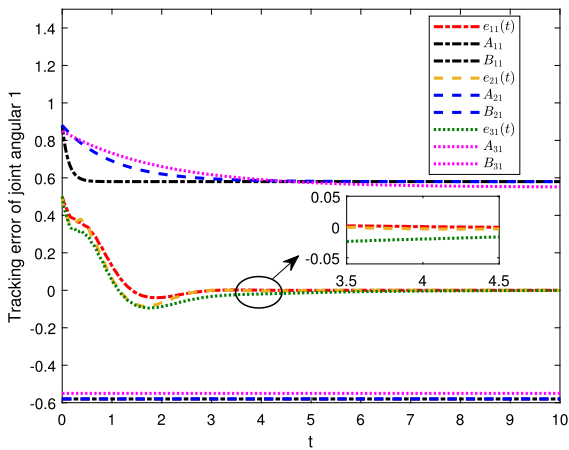


Fig. 13 Regulation index $e_1(t)$ (rad)—Case 2

Condition 2) $A_{21}(t) = -0.58, B_{21}(t) = 0.58 + 0.3e^{-1t}$ and $A_{22}(t) = -0.5 - 0.45e^{-4t}, B_{22}(t) = 0.5 + \frac{0.4}{1+t^2}$;

Condition 3) $A_{31}(t) = -0.55, B_{31}(t) = 0.55 + 0.3e^{-0.5t}$ and $A_{32}(t) = -0.5 - 0.45e^{-0.5t}, B_{32}(t) = 0.5 + \frac{0.4}{1+2t^3}$.

In order to reflect the regulation ability of the different performance functions, the above selected functions are divided into two categories, i.e., $\varrho + \mu e^{-\kappa t}$, $\frac{\kappa}{\mu + t^\varsigma}$. As for the first exponential function, $B_{i1}(t) = 0.58 + 0.3e^{-\kappa_i t}$ are chosen that varies with exponential index κ_i , which determines the convergent rate of regulation error.

From Fig. 11, the regulation convergent rate increases with the increase of exponential gain κ_i . It is clear from Fig. 12 that the convergence performance of the exponential function $\varrho + \mu e^{-\kappa t}$ is superior to fractional polynomial function $\frac{\kappa}{\mu + t^\varsigma}$. Accordingly, the regulation error of two angular positions with prescribed performance functions is displayed in Figs. 13 and 14. From Figs. 15 to 16, it indicates that the generalized mode vibration can be reduced to zero with different rates. As shown in Figs. 17, 18, 19, the vibration displacements under the above prescribed perform functions become smaller along the time axis in contrast with the fractional polynomial function.

Case 3. Novel flexible prescribed performance \mathcal{K} with input quantization

To better illustrate the efficacy of the quantized FPPC law in this case, the following control gains and performance functions are listed. $k_1 = 1.8, k_2 = 3.6, \mathcal{A}_1(t) = -0.60$ and $\mathcal{B}_1(t) = 0.60 + 0.45e^{-9t}, \mathcal{A}_2(t) =$

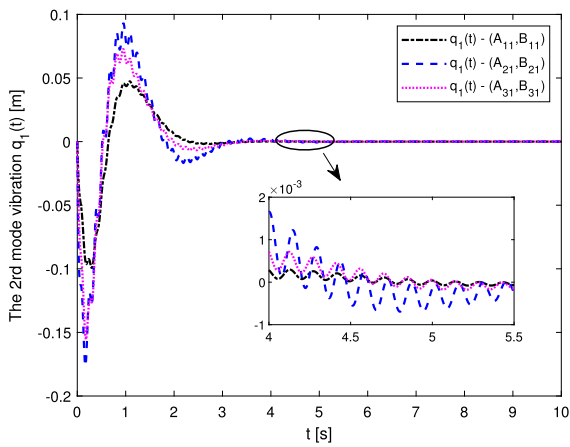


Fig. 15 1st vibration mode $q_1(t)$ (m)—Case 2

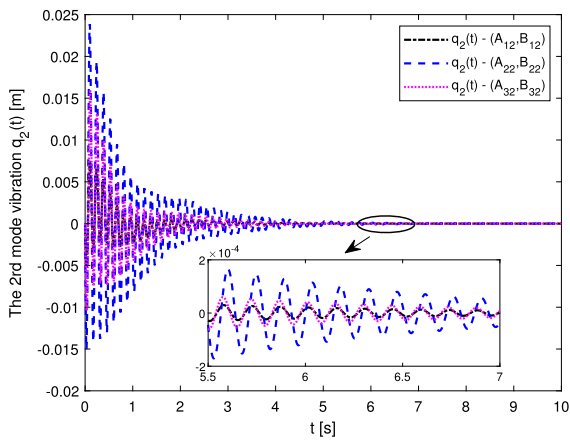


Fig. 16 2nd vibration mode $q_2(t)$ (m)—Case 2

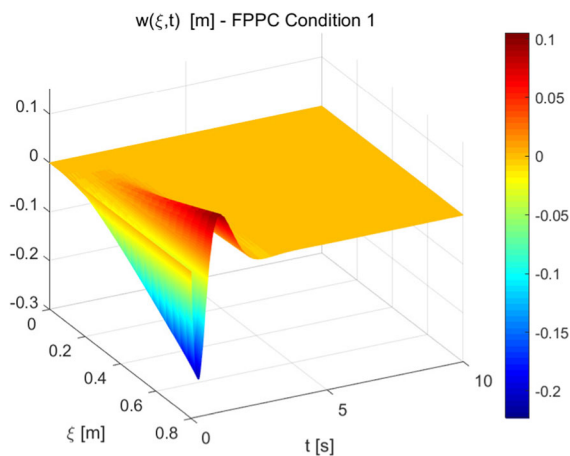


Fig. 17 The total vibration surface $w(\xi, t)$ (m) for Condition 1

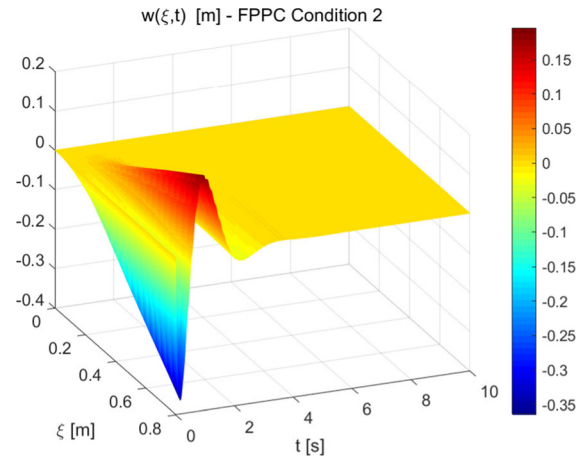


Fig. 18 The total vibration surface $w(\xi, t)$ (m) for Condition 2

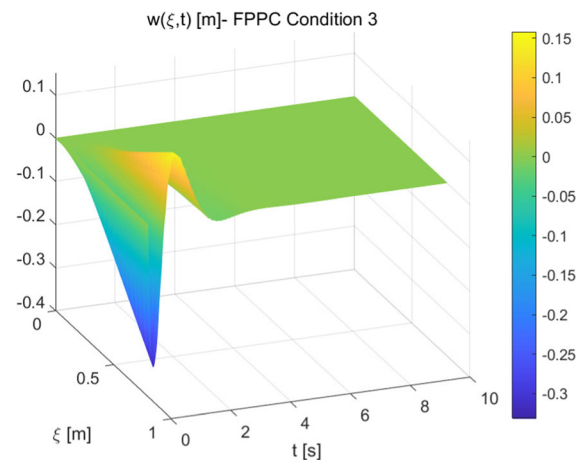


Fig. 19 The total vibration surface $w(\xi, t)$ (m) for Condition 3

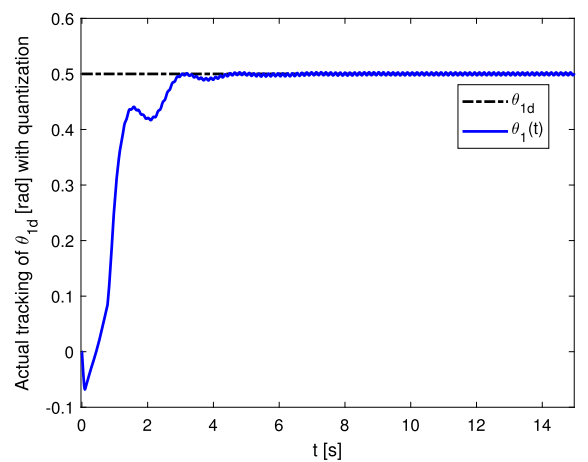


Fig. 20 Actual tracking of θ_{1d} (rad) with input quantization in Case 3

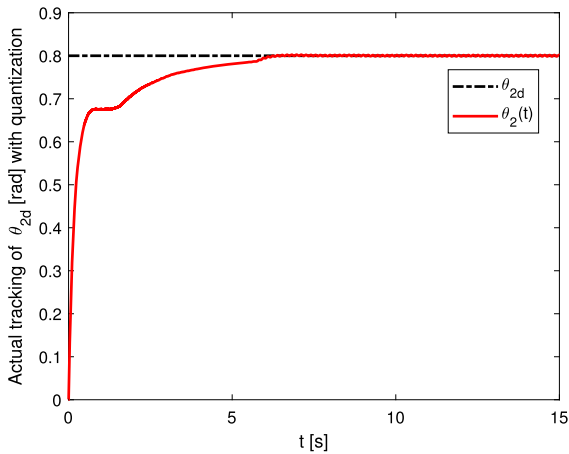


Fig. 21 Actual tracking of θ_{2d} (rad) with input quantization in Case 3

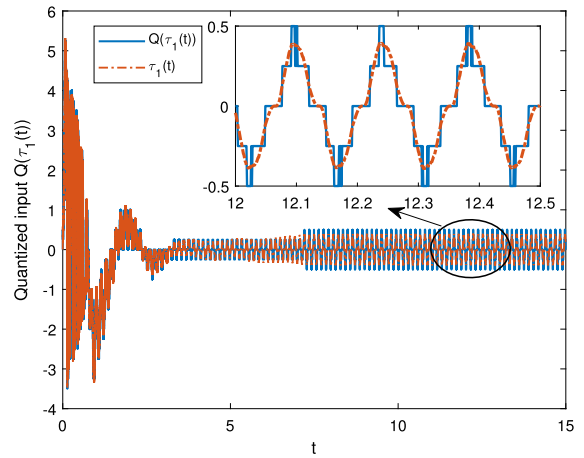


Fig. 23 Quantized input $Q(\tau_1(t))$ (Nm) in Case 3

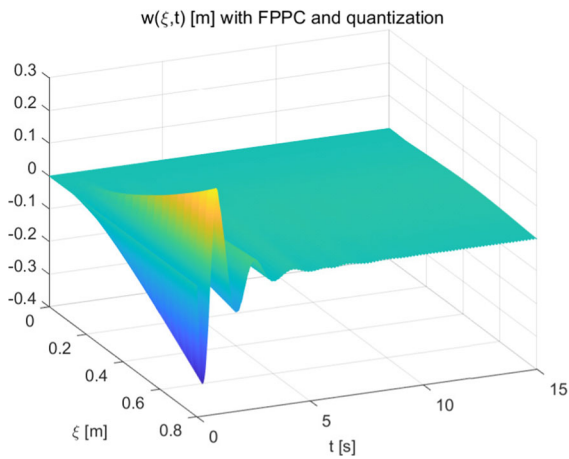


Fig. 22 The total vibration surface $w(\xi, t)$ (m) in Case 3

$-0.31 - 0.55e^{-7t}$, $B_2(t) = 0.31 + \frac{1}{2+2t^3}$, $\rho_1 = 0.025$, $\delta_1 = 0.25$, $\rho_2 = 0.01$, $\delta_2 = 0.25$, $\sigma_1 = 0.01$ and $\sigma_2 = 0.015$, $\gamma_1 = 1.6$ and $\gamma_2 = 1.8$.

Figures 20 and 21 show the regulation profiles of angular positions under the designed FPPC law with input quantization. Figure 22 represents the flexible displacement of the closed-loop RFCRSs with the quantized FPPC law. The corresponding control inputs of the RFCRSs with quantization are displayed in Figs. 23, 24. Note that the regulation errors cluster in a tiny area near zero in the presence of input quantization in Figs. 25, 26 in comparison with the regulation errors in Figs. 9, 10.

In terms of the above results, it can be concluded that, with the developed FPPC law with quantization, the

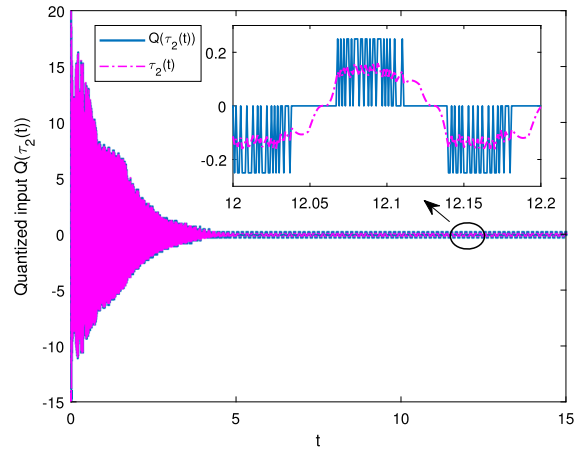


Fig. 24 Quantized input $Q(\tau_2(t))$ (Nm) in Case 3

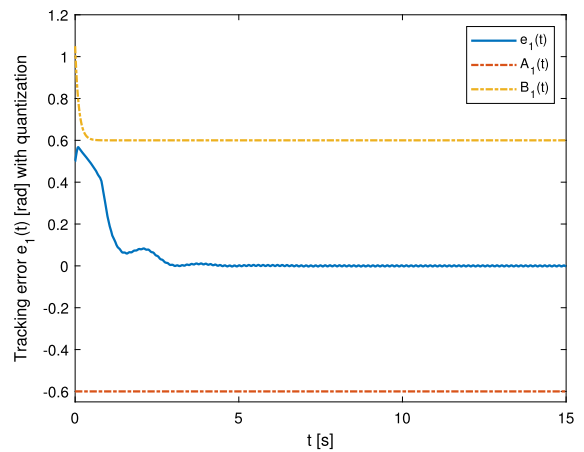


Fig. 25 Regulation $e_1(t)$ (rad) under quantization

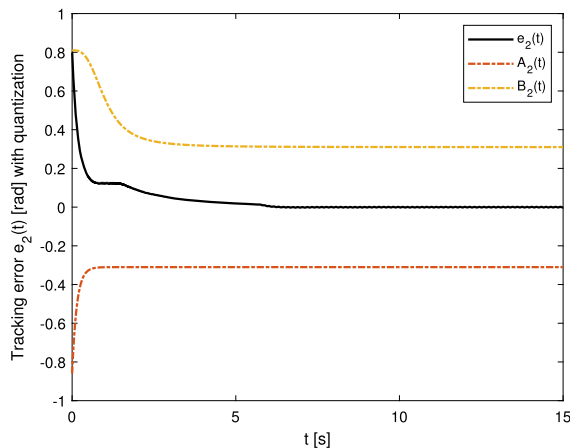


Fig. 26 Regulation $e_2(t)$ (rad) under quantization

desired angular position can be reached with flexible prescribed performance and the vibration can also be eliminated.

7 Conclusions

In this work, the model of the RFCRSs has been obtained by using the reduced-order strategy—AMM. The derived model and the flexible prescribed performance control (FPPC) law have been proposed for both with and without quantization. According to the backstepping-based Lyapunov stability method, the tracking errors of RFCRSs with the proposed FPPC laws converge to a compact set within the prescribed performance in the presence of quantization. Meanwhile, the regulation errors of the rigid–flexible robotic systems without quantization eventually converge rapidly to zero. Finally, the cases of simulation demonstrate the feasibility of the proposed flexible prescribed performance control and the input quantization has very little effect on the controlled RFCRSs with robust adaptive FPPC law. In our forthcoming work, we will explore the experimental implementation of the proposed FPPC approaches on rigid–flexible robotic systems. This will involve utilizing dSPACE-MATLAB/Simulink real-time hardware-in-the-loop control technology to validate FPPC methods.

Acknowledgements This work is partially supported by the National Natural Science Foundation of China under grant numbers [Grant Nos. 62173182, 61773212].

Funding This work is supported by the National Natural Science Foundation of China under grant numbers of 62173182, 61773212.

Data availability Data sharing not applicable to this article as no datasets were generated or analyzed during the current study.

Declarations

Conflict of interest The authors declare that they have no conflict of interest.

References

1. He, W., He, X.Y., Ge, S.S.: Boundary output feedback control of a flexible string system with input saturation. *Nonlinear Dyn.* **80**, 871–888 (2015)
2. Souza, A.G., Souza, L.C.G.: Design of a controller for a rigid–flexible satellite using the H-infinity method considering the parametric uncertainty. *Mech. Syst. Signal Proc.* **116**, 641–650 (2019)
3. Liu, Z.J., Shi, J., He, Y., Zhao, Z.J., Lam, H.K.: Adaptive fuzzy control for a spatial flexible hose system with dynamic event-triggered mechanism. *IEEE Trans. Aerosp. Electron. Syst.* **59**(2), 1156–1167 (2023)
4. Wang, Y., Yu, F.J., Li, Q.Z., Chen, Y.: Dual-space configuration synthesis method for rigid–flexible coupled cable-driven parallel mechanisms. *Ocean Eng.* **271**, 113753 (2023)
5. He, W., Meng, T.T., He, X.Y., Ge, S.Z.: Unified iterative learning control for flexible structures with input constraints. *Automatica* **96**, 326–336 (2018)
6. Tian, L.F., Collins, C.: A dynamic recurrent neural network-based controller for a rigid–flexible manipulator system. *Mechatronics* **14**(5), 471–490 (2004)
7. Lochan, K., Roy, B.K., Subudhi, B.: A review on two-link flexible manipulators. *Annu. Rev. Control* **42**, 346–367 (2016)
8. Meng, T., He, W., He, X.: Tracking control of a flexible string system based on iterative learning control. *IEEE Trans. Contr. Syst. Tech.* **29**(1), 436–443 (2021)
9. Zhou, X.Y., Tian, Y., Wang, H.P.: Neural network state observer-based robust adaptive fault-tolerant quantized iterative learning control for the rigid–flexible coupled robotic systems with unknown time delays. *Appl. Math. Comput.* **430**, 127286 (2022)
10. Zhao, Z.J., Liu, Z.J., He, W., Hong, K.S., Li, H.X.: Boundary adaptive fault-tolerant control for a flexible Timoshenko arm with backlash-like hysteresis. *Automatica* **130**, 109690 (2021)
11. Liu, Z.J., Zhao, Z., Ahn, C.K.: Boundary constrained control of flexible string systems subject to disturbances. *IEEE Trans. Circuit Syst. II Exp. Br.* **67**(1), 112–116 (2020)
12. Zhang, S., Liu, R., Peng, K., He, W.: Boundary output feedback control for a flexible two-link manipulator system with high-gain observers. *IEEE Trans. Control Syst. Tech.* **29**(2), 835–840 (2021)

13. Cao, F.F., Liu, J.K.: Boundary control for a constrained two-link rigid-flexible manipulator with prescribed performance. *Int. J. Control* **91**(5), 1091–1103 (2018)
14. Han, F., Jia, Y.: Sliding mode boundary control for a planar two-link rigid-flexible manipulator with input disturbances. *Int. J. Control Autom. Syst.* **18**, 351–362 (2020)
15. Zhao, Z.J., He, X., Ahn, C.K.: Boundary disturbance observer-based control of a vibrating single-link flexible manipulator. *IEEE Trans. Syst. Man Cyber. Syst.* **51**(4), 2382–2390 (2021)
16. Xie, D., Jian, K., Wen, W.: An element-free Galerkin approach for rigid-flexible coupling dynamics in 2D state. *Appl. Math. Comput.* **310**, 149–168 (2017)
17. Hao, T., Wang, H., Xu, F., Wang, J., Miao, Y.: Uncalibrated visual servoing for a planar two link rigid-flexible manipulator without joint-space-velocity measurement. *IEEE Trans. Syst. Man Cyber. Syst.* **52**(3), 1935–1947 (2022)
18. Meng, Q., Lai, X., Yan, Z., Wu, M.: Tip position control and vibration suppression of a planar two-link rigid-flexible underactuated manipulator. *IEEE Trans. Cyber.* **52**(7), 6771–6783 (2022)
19. Gao, H., He, W., Zhou, C., Sun, C.: Neural network control of a two-link flexible robotic manipulator using assumed mode method. *IEEE Trans. Ind. Inform.* **15**(2), 755–765 (2019)
20. Gao, H., He, W., Song, Y., Zhang, S., Sun, C.: Modeling and neural network control of a flexible beam with unknown spatiotemporally varying disturbance using assumed mode method. *Neurocomputing* **314**, 458–467 (2018)
21. Meng, Q., Lai, X., Yan, Z., Su, C.Y., Wu, M.: Motion planning and adaptive neural tracking control of an uncertain two-link rigid-flexible manipulator with vibration amplitude constraint. *IEEE Trans. Neural Netw. Learn. Syst.* **33**(8), 3814–3828 (2022)
22. Zhou, X.Y., Wang, H.P., Tian, Y., Zheng, G.: Neural network state observer-based robust adaptive iterative learning output feedback control for the rigid-flexible coupled robotic systems with unknown delays and backlash-like hysteresis. *Nonlinear Dyn.* **110**, 1515–1542 (2022)
23. Liu, Z.J., Han, Z., He, W.: Adaptive fault-tolerant boundary control of an autonomous aerial refueling hose system with prescribed constraints. *IEEE Trans. Autom. Sci. Eng.* **19**(4), 2678–2688 (2022)
24. Karayiannidis, Y., Doulgeri, Z.: Model-free robot joint position regulation and tracking with prescribed performance guarantees. *Robot Auton. Syst.* **60**(2), 214–226 (2012)
25. Bechlioulis, C.P., Rovithakis, A.: Adaptive control with guaranteed transient and steady state tracking error bounds for strict feedback systems. *Automatica* **45**(6), 532–538 (2016)
26. Kostarigka, A.K., Doulgeri, Z., Rovithakis, G.A.: Prescribed performance tracking for flexible joint robots with unknown dynamics and variable elasticity. *Automatica* **49**(5), 1137–1147 (2013)
27. Shao, X., Hu, Q., Shi, Y., Jiang, B.: Fault-tolerant prescribed performance attitude tracking control for spacecraft under input saturation. *IEEE Trans Control Syst. Tech.* **28**(2), 574–582 (2020)
28. Dimanidis, I.S., Bechlioulis, C.P., Rovithakis, G.A.: Output feedback approximation-free prescribed performance tracking control for uncertain MIMO nonlinear systems. *IEEE Trans. Autom. Control* **65**(12), 5058–5069 (2020)
29. Jia, F.J., Wang, X.H., Zhou, X.Y.: Robust adaptive prescribed performance control for a class of nonlinear pure-feedback systems. *Int. J. Robust Nonlinear Control* **29**, 3971–3987 (2019)
30. Liu, A., Yu, L., Zhang, W., Chen, M.Z.Q.: Moving horizon estimation for networked systems with quantized measurements and packet dropouts. *IEEE Trans. Circuits Syst. I Reg. Pap.* **60**(7), 1823–1834 (2013)
31. Wang, C.L., Wen, C.Y., Lin, Y., Wang, W.: Decentralized adaptive tracking control for a class of interconnected nonlinear systems with input quantization. *Automatica* **81**, 359–368 (2017)
32. Brockett, R.W., Liberzon, D.: Quantized feedback stabilization of linear systems. *IEEE Trans. Autom. Control.* **45**(7), 1279–1289 (2000)
33. Yao, D.Y., Li, H.Y., Shi, Y.: Adaptive event-triggered sliding mode control for consensus tracking of nonlinear multi-agent systems with unknown perturbations. *IEEE Trans. Cybern.* **53**(4), 2672–2684 (2023)
34. Xing, L., Wen, C., Zhu, Y., Su, H.: Output feedback control for uncertain nonlinear systems with input quantization. *Automatica* **65**, 191–202 (2016)
35. Zhao, X.N., Zhang, S., Liu, Z.J., Wang, J., Gao, H.B.: Adaptive event-triggered boundary control for a flexible manipulator with input quantization. *IEEE/ASME Trans. Mechatron.* **27**(5), 3706–3716 (2021)
36. Ji, N., Liu, J.K.: Adaptive boundary control for flexible three-dimensional Euler-Bernoulli beam with input signal quantization. *Int. J. Adapt. Control Signal Process.* **32**, 1162–1181 (2018)
37. Cao, F.F., Liu, J.K.: Boundary vibration control for a two-link rigid-flexible manipulator with quantized input. *J. Vib. Control* **25**(23–24), 2935–2945 (2019)
38. Yao, D.Y., Li, H.Y., Shi, Y.: Event-based average consensus of disturbed MASs via fully distributed sliding mode control. *IEEE Trans. Autom. Control* (2023). <https://doi.org/10.1109/TAC.2023.3317505>
39. Yigit, A.S.: On the stability of PD control for a two-link rigid-flexible manipulator. *J. Dyn. Syst. Meas. Control* **116**(2), 208–215 (1994)

Publisher's Note Springer Nature remains neutral with regard to jurisdictional claims in published maps and institutional affiliations.

Springer Nature or its licensor (e.g. a society or other partner) holds exclusive rights to this article under a publishing agreement with the author(s) or other rightsholder(s); author self-archiving of the accepted manuscript version of this article is solely governed by the terms of such publishing agreement and applicable law.